Article

Current Biology

Activation of a Plant NLR Complex through Heteromeric Association with an Autoimmune Risk Variant of Another NLR

Graphical Abstract

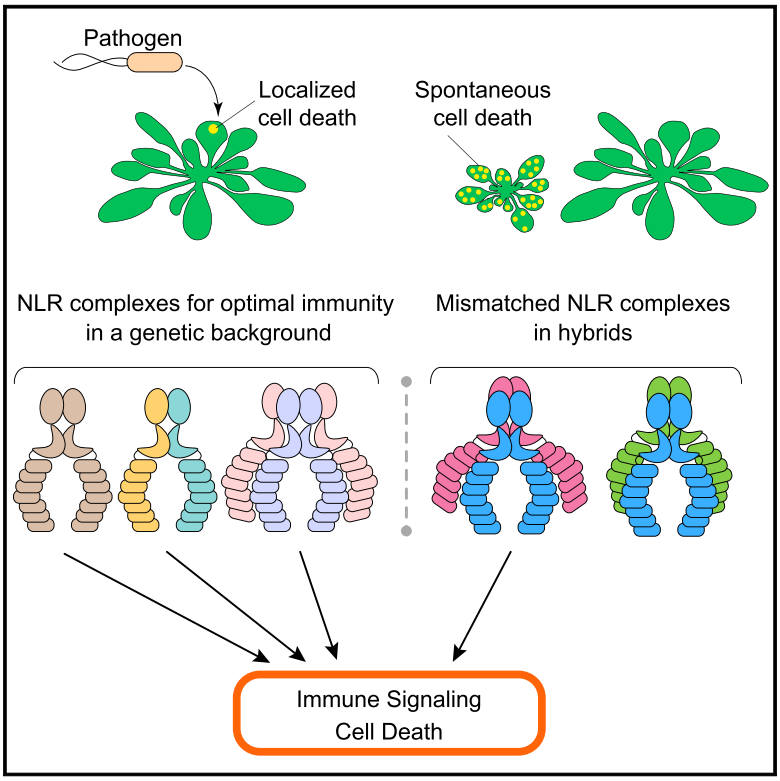

Authors

Diep T.N. Tran, Eui-Hwan Chung, Anette Habring-Müller, ..., Jeffery L. Dangl, Detlef Weigel, Eunyoung Chae

Correspondence

weigel@weigelworld.org (D.W.), eunyoung.chae@tue.mpg.de (E.C.)

In Brief

Mismatched combinations of plant immune proteins can trigger autoimmunity in hybrids. Tran, Chung et al. report that a pair of NLR immune receptor variants, encoded by unlinked loci, triggers autoimmunity through heteromeric association. Signaling activity of the NLR complex depends on the sum of activation potentials of individual partner NLRs.

Highlights

- Two unlinked plant NLRs physically interact to trigger autoimmunity
- The N-terminal TIR domains mediate heteromeric NLR association
- NLR multimerization is not sufficient for signaling

Tran et al., 2017, Current Biology *27*, 1–13
April 24, 2017
http://dx.doi.org/10.1016/j.cub.2017.03.018

CellPress

Please cite this article in press as: Tran et al., Activation of a Plant NLR Complex through Heteromeric Association with an Autoimmune Risk Variant of Another NLR, Current Biology (2017), http://dx.doi.org/10.1016/j.cub.2017.03.018

Current Biology
Article

Activation of a Plant NLR Complex through Heteromeric Association with an Autoimmune Risk Variant of Another NLR

Diep T.N. Tran,[1,6] Eui-Hwan Chung,[2,3,6] Anette Habring-Müller,[1] Monika Demar,[1] Rebecca Schwab,[1] Jeffery L. Dangl,[2,3,4,5] Detlef Weigel,[1,7,*] and Eunyoung Chae[1,*]
[1]Department of Molecular Biology, Max Planck Institute for Developmental Biology, 72076 Tübingen, Germany
[2]Department of Biology, University of North Carolina, Chapel Hill, NC 27599, USA
[3]Howard Hughes Medical Institute, University of North Carolina, Chapel Hill, NC 27599, USA
[4]Curriculum in Genetics and Molecular Biology, Carolina Center for Genome Sciences, Chapel Hill, NC 27599, USA
[5]Department of Microbiology and Immunology, University of North Carolina, Chapel Hill, NC 27599, USA
[6]Co-first author
[7]Lead Contact
*Correspondence: weigel@weigelworld.org (D.W.), eunyoung.chae@tue.mpg.de (E.C.)
http://dx.doi.org/10.1016/j.cub.2017.03.018

SUMMARY

When independently evolved immune receptor variants meet in hybrid plants, they can activate immune signaling in the absence of non-self recognition. Such autoimmune risk alleles have recurrently evolved at the *DANGEROUS MIX2* (*DM2*) nucleotide-binding domain and leucine-rich repeat (NLR)-encoding locus in *A. thaliana*. One of these activates signaling in the presence of a particular variant encoded at another NLR locus, *DM1*. We show that the risk variants of DM1 and DM2d NLRs signal through the same pathway that is activated when plant NLRs recognize non-self elicitors. This requires the P loops of each protein and Toll/interleukin-1 receptor (TIR)-domain-mediated heteromeric association of DM1 and DM2d. DM1 and DM2d each resides in a multimeric complex in the absence of signaling, with the DM1 complex shifting to higher molecular weight when heteromerizing DM2 variants are present. The activation of the DM1 complex appears to be sensitive to the conformation of the heteromerizing DM2 variant. Autoimmunity triggered by interaction of this NLR pair thus suggests that activity of heteromeric NLR signaling complexes depends on the sum of activation potentials of partner NLRs.

INTRODUCTION

The ability to discriminate non-self from self is essential for effective immunity. In plants and mammals, nucleotide-binding domain and leucine-rich repeat (NLR)-containing receptors have convergently evolved crucial roles in recognition of non-self and modified-self molecules as danger signals [1]. In plants, NLRs can directly associate with pathogen-derived effectors, or they can indirectly sense effector-mediated modification of other host proteins. Some of these are so-called NLR guardees, proteins that are targeted by effectors because their suppression enhances virulence, whereas others are decoys that merely entrap effectors and that have no direct function in host resistance [2, 3]. Upon recognition, plant NLRs are thought to undergo nucleotide-dependent conformation changes, most likely by relieving autoinhibitory intramolecular contacts [4]. This in turn exposes the N-terminal coiled-coil (CC) or Toll/interleukin-1 receptor (TIR) domain for participation in higher-order signaling complexes [5–10].

NLR domains that directly engage pathogen effectors, such as the leucine-rich repeat (LRR) domain, are highly diverse, reflecting effector-NLR co-evolution [11, 12]. Binding specificity for effector variants translates into a matching recognition spectrum of NLRs, with contributions mainly, but not exclusively, from LRR domains [12–15]. Extensive structure-function studies have shown that the different domains have to be finely matched for optimal specificity and robustness of NLR signaling. In agreement, minor changes can drastically alter the activity and specificity of NLR variants [16–18], and swapping even a small domain between variants can trigger severe autoimmunity [19, 20].

One way to increase specificity without compromising the strength of an immune response is to partition recognition and signaling functions into distinct NLRs. In several examples of such pairs, one partner signals whereas the other no longer needs a functional P loop, but has an extra domain that directly interacts with effectors [21–24]. Pairs functionally characterized to date are encoded by adjacent genes at the same genomic locus, but a few NLR pairs encoded by unlinked loci function in a similar manner. In mammals, NAIP and NLRC4 NLRs serve as co-receptors, with different NAIP isoforms sensing distinct, conserved pathogen molecules and NLRC4 mainly transducing signals [25, 26]. In plants, several NLRs, such as tobacco NRG1, *Solanaceae* NRC1-like proteins, and *A. thaliana* ADR1 proteins, mediate signaling from unlinked, effector-sensing NLRs [27–30], although it is not known whether these NLRs reside in the same complex.

Given the demands placed on an immune system that has to detect and rapidly respond to a multitude of pathogens, it may not come as a surprise that things can go wrong, and sometimes very badly so. This is the case in some hybrid plants, where independently evolved immune system components are mismatched

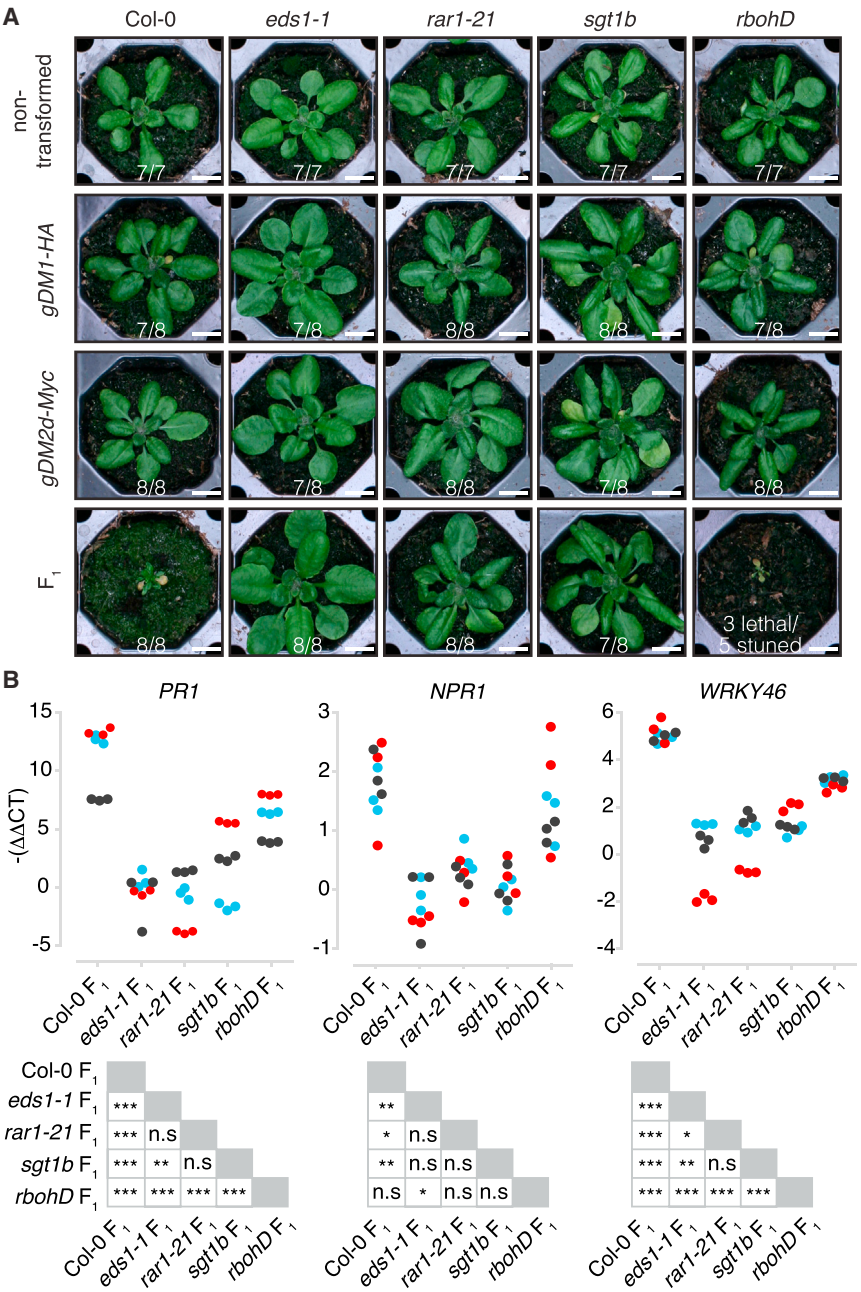

Figure 1. Genetic Requirement for DM1/DM2d-Dependent Autoimmunity

(A) Rosettes of 30-day-old *A. thaliana* plants expressing *gDM1-HA*, *gDM2d-Myc*, or both (F_1) in the indicated backgrounds. The numbers indicate the proportion of the presented phenotype in three sowings. Scale bars, 1 cm.

(B) Expression analysis of immunity marker genes *PR1*, *NPR1*, and *WRKY46*. Relative expression of each marker gene in F_1 hybrids is indicated as $-(\Delta\Delta CT)$ values from three biological replicates (different color dots), with three technical replicates (one dot for each data point). Tukey's multiple comparison test was used to test for statistical significance (alpha = 0.05). ***p < 0.0001, **p < 0.001, *p < 0.01; ns, p > 0.05, non-significant.

See also Figure S1 and Table S1.

We demonstrate that the autoimmune risk $DM1^{Uk\text{-}3}$ and $DM2d^{Uk\text{-}1}$ (hereafter DM1 and DM2d) NLRs associate and form an autoimmune signaling complex in planta. Because the association between DM1 and DM2g, a close paralog of DM2d, also from Uk-1, fails to trigger signaling, we propose that signaling activity depends on the conformation of the heteromerizing NLR to a DM1 oligomer complex. This autoactive heteromeric NLR complex, which does not require an effector trigger, provides a unique experimental paradigm for investigating NLR signaling.

RESULTS

Genetic Requirements for DM1/DM2d-Triggered Autoimmunity

To better understand how *DM1/DM2d*-triggered autoimmunity relates to NLR/effector-stimulated immune responses, we examined the effects of mutations in several regulators of NLR-mediated cell death. EDS1 can act by direct association with TNLs [37, 38], whereas an HSP90-, SGT1-, and RAR1-containing chaperone complex has several roles in immunity, including regulation of NLR protein stability [39]. The NADPH oxidase RBOHD modulates the spread of NLR-induced cell death through its role in generating reactive oxygen species (ROS) [40, 41]. To test the effects of mutations in *EDS1*, *SGT1B*, *RAR1*, and *RBOHD*, we generated wild-type or mutant plants (Table S1) that were homozygous for *gDM1-2xHA* (*gDM1-HA*) or *gDM2d-4xMyc* (*gDM2d-Myc*) transgenes. We combined the two transgenes in each of the five backgrounds through crosses. The F_1 progeny were grown at 16°C, a temperature at which hybrid necrosis is strongly expressed. The control F_1 hybrid plants were very small and their leaves had many necrotic spots, similar to F_1 hybrids of the Uk-1 and Uk-3 accessions, the donors of the *DM1* and *DM2d* genes (Figures 1A and

and trigger inappropriate immune reactions in the absence of pathogens. Because cell death is a typical symptom, this syndrome is known as hybrid necrosis [31]. Hybrid necrosis is often caused by interacting alleles at two unlinked loci, and alleles from complex NLR loci are the most common cause [32–35]. An example where both interacting alleles encode NLR variants is provided by the unlinked TIR-NLR (TNL) loci *DANGEROUS MIX1* (*DM1*) from *A. thaliana* accession Uk-3 and *DM2* from Uk-1. Both accessions were collected in Umkirch, Germany [32, 36]. *DM2*, which is part of the *RPP1* supercluster involved in direct recognition of ATR1 effectors [15], recurrently generates hybrid necrosis risk alleles that can also interact with non-NLR alleles [34, 36].

S1A) [32], demonstrating that the C-terminal epitopes did not interfere with DM1 and DM2d activity.

Mutations in *EDS1*, *RAR1*, and *SGT1B* almost completely suppressed the hybrid necrosis symptoms (Figure 1A), which was accompanied by greatly reduced expression of the immunity markers *PR1*, *NPR1*, and *WRKY46* (Figure 1B). In contrast, the *rbohD* mutation did not suppress the phenotype, and even occasionally enhanced the necrosis symptoms (Figure 1A). Expression of the marker genes *PR1* and *WRKY46* was much less reduced than in the other mutants (Figure 1B). *gDM1-HA/− gDM2d-Myc/− rbohD* plants were extremely stunted and failed to produce seeds, whereas *gDM1-HA/− gDM2d-Myc/−* control plants eventually set seeds, despite reduced growth and tissue necrosis (Figure S1B).

DM1/DM2d signaling thus requires factors used by other TNLs after pathogen recognition, such as EDS1 and the HSP90/SGT1B/RAR1 chaperone complex. DM1/DM2d signaling, however, does not require RBOHD-dependent ROS bursts, a result reminiscent of the *lesion simulating disease 1* (*lsd1*) mutant, whose phenotype depends on the atypical NLR ADR1-L2 [40].

Requirement of Full-Length Proteins with Functional P Loops

A convenient platform for testing NLR activities is transient expression in *Nicotiana benthamiana*. Co-expression of full-length DM1 and DM2d can induce a robust, pathogen-independent hypersensitive response (HR) in this system [36]. Because N-terminal fragments of several plant TNLs can trigger HR on their own in *N. benthamiana* [42], we also tested DM1 and DM2d fragments. Four fragments each—the TIR, TIR plus partial NB, TIR-NB and extended ARC, and LRR domains (Figures 2A and 2B)—were epitope tagged and expressed in *N. benthamiana*, with β-glucuronidase (GUS) expression as negative control. The combination of full-length DM1-HA with DM2d-Myc caused confluent cell death 4 days post-infiltration (dpi) (Figure S1C), similar to the non-epitope-tagged proteins [36]. Unlike the combination of DM1 and DM2d full-length proteins, none of the fragments on their own were sufficient to trigger HR, despite robust protein accumulation (Figures S1D and S1E). We did not observe any HR either when combinations of the DM1 and DM2d fragments were co-expressed (Figure S1C). The requirement of full-length paired proteins thus differentiates DM1/DM2d-dependent signaling from several unusual NLRs, whose N-terminal domains alone are sufficient to trigger full or partial HR [5, 7, 9, 10, 15, 42].

P loop mutations render many NLRs inactive [4]. In addition, NLR activity is altered by mutations of the MHD motif, presumably because such mutations change local conformation around the ATP-binding pocket [43, 44]. In particular, a change from MHD to MHV causes several NLRs to preferentially bind ATP, and thereby makes them constitutively active [43, 45].

To investigate whether DM1/DM2d signaling depends on P loop activity, we mutated the GIGKTT motif in DM1 and DM2d to GIAATT (Figures 2A and 2B). To quantify DM1/DM2d signaling, we established an ethanol-inducible system for DM1-HA expression (*indDM1-HA*) in *N. benthamiana* (see the Supplemental Experimental Procedures), with inducible GFP as a control. As a proxy for cell death, we measured ion leakage. We observed confluent HR 3 days after ethanol induction of DM1-HA when DM2d-Myc was co-expressed from its native promoter (Figures 2A and 2B), validating the system. We began to measure ion leakage before cell death became apparent, and stopped measurements when ion leakage plateaued after about 22 hr (Figures 2C and 2D). When DM1 or DM2d P loop mutants were co-expressed with their wild-type partner, HR was abolished (Figures 2A and 2B). Ion-leakage kinetics with the mutant versions were similar to controls (Figures 2C and 2D).

Turning to the MHD-like motifs (MHH in DM1 and MHT in DM2d), we found that, different from other systems [43, 45], neither MHV variant was constitutively active on its own (Figures 2A–2D), and both MHV variants behaved comparable to their wild-type counterparts when co-expressed with the partner NLR (Figures 2C and 2D). Furthermore, the MHD-to-MHV substitution could not overcome the loss of activity due to P loop mutations (Figures 2C and 2D). Protein blots confirmed that mutant proteins were expressed at levels comparable to wild-type versions (Figures 2E and 2F). We conclude that DM1/DM2d signaling requires the P loops of both NLRs. In addition, neither single NLR can provide full activity, because both are resistant to MHV mutations, which render other NLRs constitutively active, presumably by shifting the ratio of ATP and ADP bound at the P loop [18].

Homotypic DM1 Association and Heterotypic DM1/DM2d Association

Signaling from some plant NLRs involves homo- or heteromerization, with the N-terminal TIR or CC domains providing dimerization interfaces [5–7, 9, 10, 21, 22]. To examine DM1-DM2d protein interactions, we began with yeast-two hybrid (Y2H) assays, often used to study plant NLRs [22]. A DM1 fragment that included the TIR and partial NB domain (TIR-pNB) interacted both with full-length DM1 and with three TIR-containing DM1 fragments (Figure 3A). DM1 TIR-pNB also interacted, albeit more weakly, with DM2d TIR and TIR-pNB fragments (Figure 3A). Neither the LRR fragments of DM1 and DM2d nor full-length DM2d showed evidence of interaction, possibly due to insufficient protein accumulation (Figures 3A and S2A). We did not detect DM2d self-association in yeast, also most likely because of insufficient protein accumulation (Figures S2B and S2C). We conclude that the N termini of DM1 and DM2d provide an interface for homo- and/or heterotypic interactions.

We confirmed the Y2H results with transient co-expression of *gDM1-Myc* and either *gDM1-HA* or *gDM2d-HA* in *N. benthamiana* (Figures 3B and 3C). Co-immunoprecipitation demonstrated that DM1-Myc could associate with both DM1-HA and DM2d-HA (Figure 3C, lanes 5 and 6). DM1-HA was much more efficiently co-immunoprecipitated than DM2d-HA, even though DM2d-HA was expressed at higher levels (Figure 3C, compare inputs). The difference may reflect a different stoichiometry of DM1 and DM2d in the signaling complex or differences in the binding affinity between DM proteins, but it might also have a more trivial explanation, with DM1/DM2d complexes being depleted because of rapid death of cells containing both proteins. Nonetheless, our data indicate strong DM1 self-association, and DM1/DM2d association. We also detected DM2d-HA/DM2d-Myc complexes (Figure 3C, lane 7), indicating that, like DM1, DM2d can self-associate.

We further confirmed the interaction between DM1 and DM2d using an *A. thaliana* F_1 progeny of lines that expressed

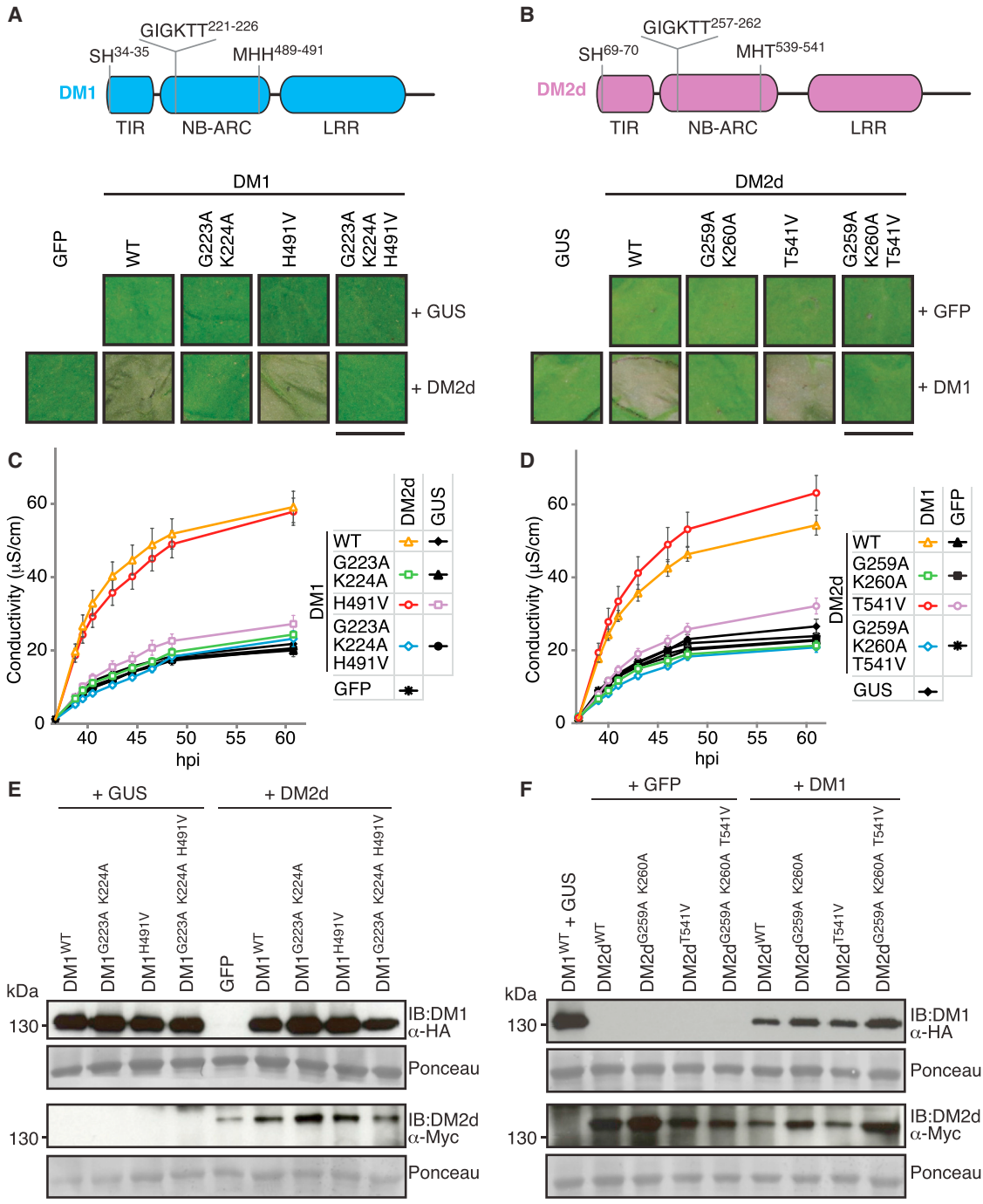

Figure 2. Contribution of P Loop Function to DM1/DM2d Signaling

(A and B) Images of *N. benthamiana* leaves transiently co-expressing ethanol-induced DM1 variants with wild-type DM2d (A), and DM2d variants with ethanol-induced wild-type DM1 (B). Images were taken after 36 hr of ethanol induction. Scale bar, 1 cm. Schematic diagrams of DM1 and DM2d with positional information are at the top.

(C and D) Ion leakage as an indication of HR in plants shown in (A) and (B). Values are means ± SEM (n = 8). hpi, hours post-infiltration.

(E and F) Protein blots for the experiments shown in (A) and (B), with samples taken 12 hr after ethanol induction. Ponceau-S staining is shown to indicate loading. IB, immunoblotting.

indDM1-HA and *gDM2d-Myc*. The expression of DM1-HA was induced with ethanol in 15-day-old seedlings grown at 23°C. Whereas non-induced F_1 and parents carrying the individual transgenes did not show HR symptoms, ethanol-treated individuals from six independent F_1 lines became necrotic (Figure 3D, red arrowheads). When we analyzed leaf samples from the treated F_1 individuals in bulk, we could readily detect DM2d-Myc after pull-down with DM1-HA (Figure 3E). This result is

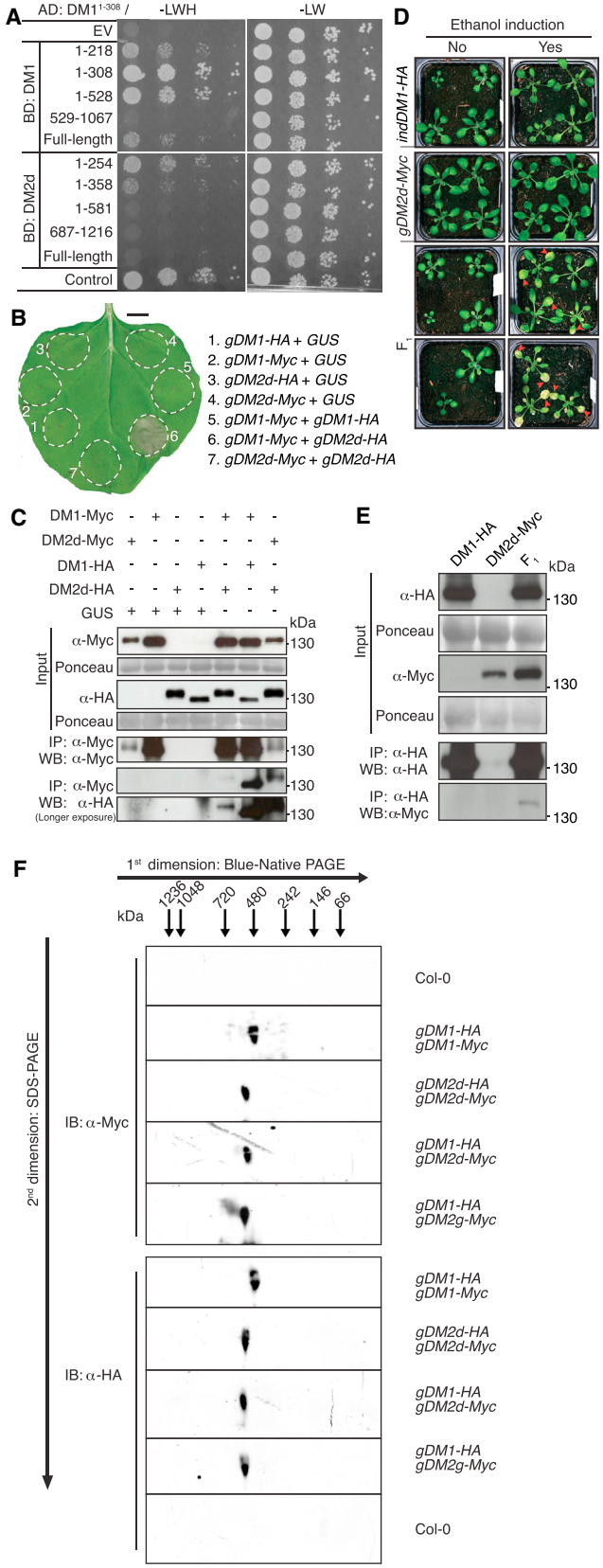

Figure 3. Homo- and Heterotypic Association of DM1 and DM2d

(A) Y2H assays to define interaction interfaces. Serial dilutions were used to visualize interaction strengths on −LWH (leucine tryptophan histidine) medium. AD-RGL3 and BD-AP1 fusions were used as positive controls. AD, GAL4 activation domain; BD, GAL4 DNA-binding domain; EV, empty vector. See the Supplemental Experimental Procedures for details.

(B) HR in *N. benthamiana* triggered by DM1-Myc and DM2d-HA combinations (4 dpi) used for the co-immunoprecipitation experiments in (C). Scale bar, 1 cm.

(C) Co-immunoprecipitation analysis with protein extracts from *N. benthamiana* leaf samples (B) collected at 2 dpi. 10% of input is shown as a pre-co-immunoprecipitation control. IP, immunoprecipitation; WB, western blot.

(D) Hybrid necrosis in F_1 plants carrying *indDM1-HA* and *gDM2d-Myc* in Col-0 background after 3 days of ethanol induction. Red arrowheads indicate necrotic symptoms, which were only observed in F_1 plants upon induction.

(E) Co-immunoprecipitation analysis with protein extracts from *A. thaliana* samples (D) collected 18 days after ethanol induction. 10% of input is shown as a pre-co-immunoprecipitation control.

(F) Blue native-PAGE showing higher-order oligomerization of DM1, DM2d, and DM1/DM2d,g complexes in *A. thaliana* F_1 hybrids carrying the indicated constructs on the right.

See also Figure S2.

consistent with both Y2H and *N. benthamiana* co-immunoprecipitation data.

We used blue native-PAGE to investigate the composition of DM1 and DM2d complexes in *A. thaliana*. Both DM1-HA and DM1-Myc proteins were found in a complex of approximately 500 kDa, whereas DM2d proteins were in an even larger complex (Figure 3F). In extracts from plants expressing both proteins, DM1-HA and DM2d-Myc co-migrated, both being detected in a complex that was larger than what we saw for DM1 alone (Figure 3F). A similar increase in complex size was observed when plants expressed both DM1-HA and DM2g-Myc (Figure 3F), a combination that does not trigger autoimmunity [36]. These results suggest that DM2 molecules may alter existing DM1 complexes through heterotypic interactions but that only the DM2d variant forms a heteromeric complex with DM1 that triggers autoimmunity.

DM1/DM2d Association and Signaling

Crystal structures of RPS4 and RRS1 NLRs have revealed two important residues, Ser and His (SH motif), at the hetero- and homodimeric interfaces of their TIR domains [22]. We therefore tested whether the SH motifs of DM1 and DM2d are critical for their physical association. In Y2H assays, SH mutations compromised both homo- and heterotypic interactions (Figures 4A and S3A), suggesting that the DM1 and DM2d TIR domains make contacts similar to those of RPS4 and RRS1 [22]. The SH motif in DM2d was essential for HR in *N. benthamiana* (Figures 4B, S3B, and S3C). Mutations at the SH motif of DM1 also compromised HR in *N. benthamiana*, but a few cell-death foci were still apparent (Figures 4B, S3B, and S3C), which might be due to a possible contribution from an additional interface in the TIR domain to signaling [5, 7, 46–48].

In the RPS4/RRS1 pair, residues close to the SH motif, such as R30 in RPS4, also affect their interaction [22]. We introduced a series of substitutions at the corresponding position in DM1 (G31) and DM2d (T66). In DM1, changes to negatively charged residues (G31D or G31E), but not to positively charged or polar residues (G31R or G31T), reduced homo- and heterotypic Y2H

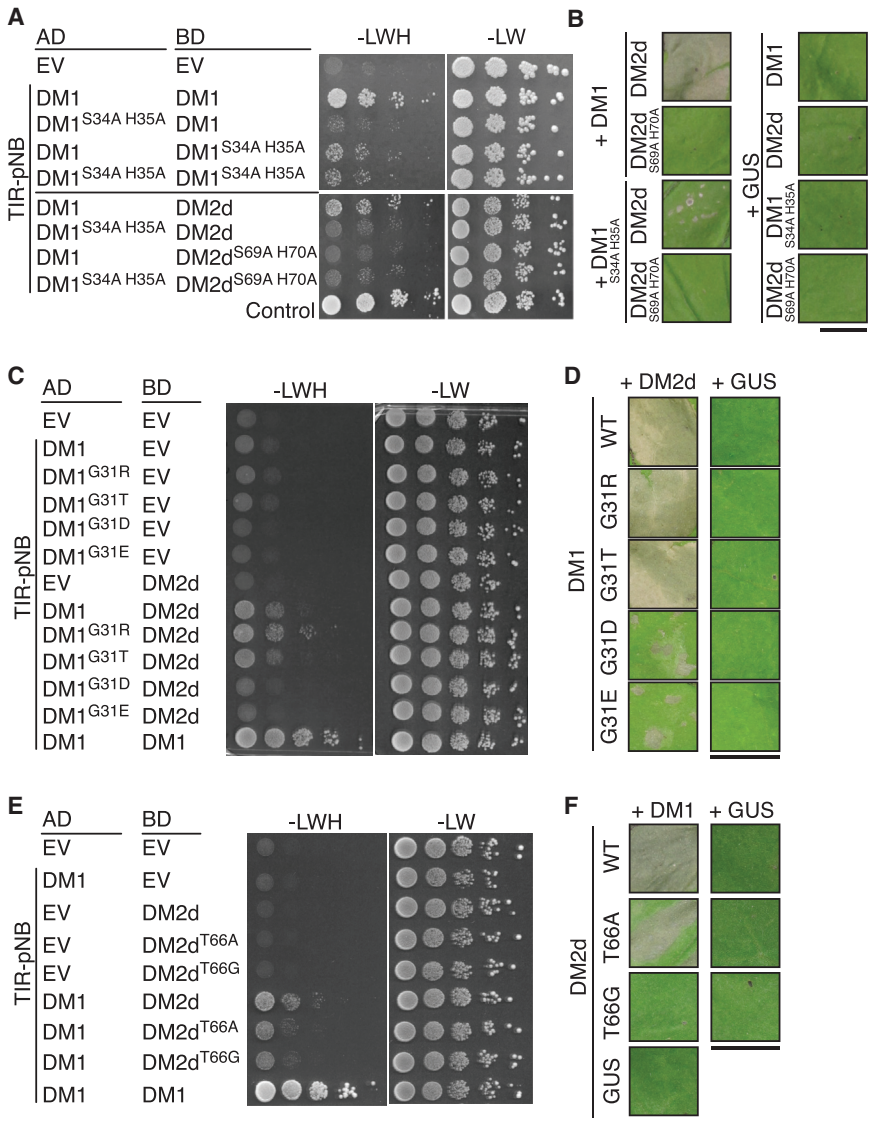

Figure 4. Heterotypic Interaction and DM1/DM2d Signaling

(A) Y2H assays of TIR-pNB fragments of DM1 ($DM1^{1–308}$) and DM2d ($DM2^{1–358}$) with mutations in SH motif. See Figure 3A legend for details of Y2H.

(B) HR in *N. benthamiana* triggered by mutant DM1 and DM2d combinations (4 dpi).

(C) Y2H assays of TIR-pNB fragments of DM1 G31 variants and $DM2d^{WT}$.

(D) HR in *N. benthamiana* triggered by DM1 G31 variants and $DM2d^{WT}$ (4 dpi).

(E) Y2H assays of TIR-pNB fragments of DM2d T66 variants and $DM1^{WT}$.

(F) HR in *N. benthamiana* triggered by $DM1^{WT}$ and DM2d T66 variants (4 dpi).

Scale bars, 1 cm (B, D, and F). See also Figure S3.

interactions (Figures 4C, S3D, and S3E) and HR in *N. benthamiana* (Figures 4D and S3F). In DM2d, both T66A and T66G mutations affected the strength of heteromeric interaction with DM1 in the Y2H assay (Figures 4E and S3G), with T66G eliminating, and T66A reducing, HR in *N. benthamiana* (Figures 4F and S3H).

Our experiments with variants that have mutations in or near the N-terminal SH motif in the TIR domains thus demonstrate that physical interactions at the TIR interface between DM1 and DM2 correlate with autoimmune signaling and that the stability of the interface appears to quantitatively affect signaling output.

DM1/DM2g Association and Lack of Signaling

Because the interaction interfaces of TNLs generally are in the TIR domain, we asked whether DM2d homologs with highly similar TIR domains can associate with DM1. The closest paralog of DM2d in the same genome is DM2g, with 95% amino acid similarity in the TIR domain. Similar to DM2d, DM2g weakly associates with DM1 in a Y2H assay (Figure 5A), apparently also through the N terminus (Figure S4A). The DM1 TIR-pNB fragment can similarly associate with the TIR-pNB fragment of RPP1 WsA, although not of other DM2h-type RPP1 homologs (Figures 5B and S4B), suggesting that the DM1 TIR domain can interact with TIR domains from a certain range of DM2/RPP1 proteins (Figure S5A). To confirm that failure of the DM2g/DM1 combination to trigger immune signaling [36] is not due to insufficient DM2g accumulation, we expressed *DM2g* not only from the *DM2g* or *DM2d* promoters but also from the cauliflower mosaic virus 35S promoter. None triggered HR in *N. benthamiana* in combination with DM1 (Figure 5C), even when protein levels were high (Figure 5D). We conclude that physical association of DM2 paralogs with DM1 is insufficient for immune signaling.

To further define the functional domains determining DM2d activity, we tested a series of *DM2d* promoter-driven DM2d/DM2g chimeras in *N. benthamiana*. Differences between DM2d and DM2g reside mostly in the TIR and LRR domains and the extended C-terminal region (Figure 5E, top panel). Replacement of either the TIR or LRR domain rendered DM2d inactive (Figure S4C, TIR swap 1 and LRR swap 2), whereas introducing either the DM2d TIR or LRR domain into DM2g was insufficient to trigger HR in combination with DM1 (Figure S4C, TIR swap 2 and LRR swap 1). Replacing the DM2d NB-ARC domain with that from DM2g did not inactivate DM2d (NB-ARC swap 1), whereas the reverse chimera (NB-ARC swap 2) was inactive (Figures S4C and S4E). The swapping results thus suggest that the TIR and LRR domains together determine DM2d-like properties.

To further narrow down the LRR region that functions in concert with the TIR domain in DM2d, we used the DM2d chimera with the $NB\text{-}ARC^{DM2g}$ domain (Figure 5E, NB-ARC swap 1) as a backbone and generated additional chimeras in which DM2d LRR segments were successively replaced by ones from

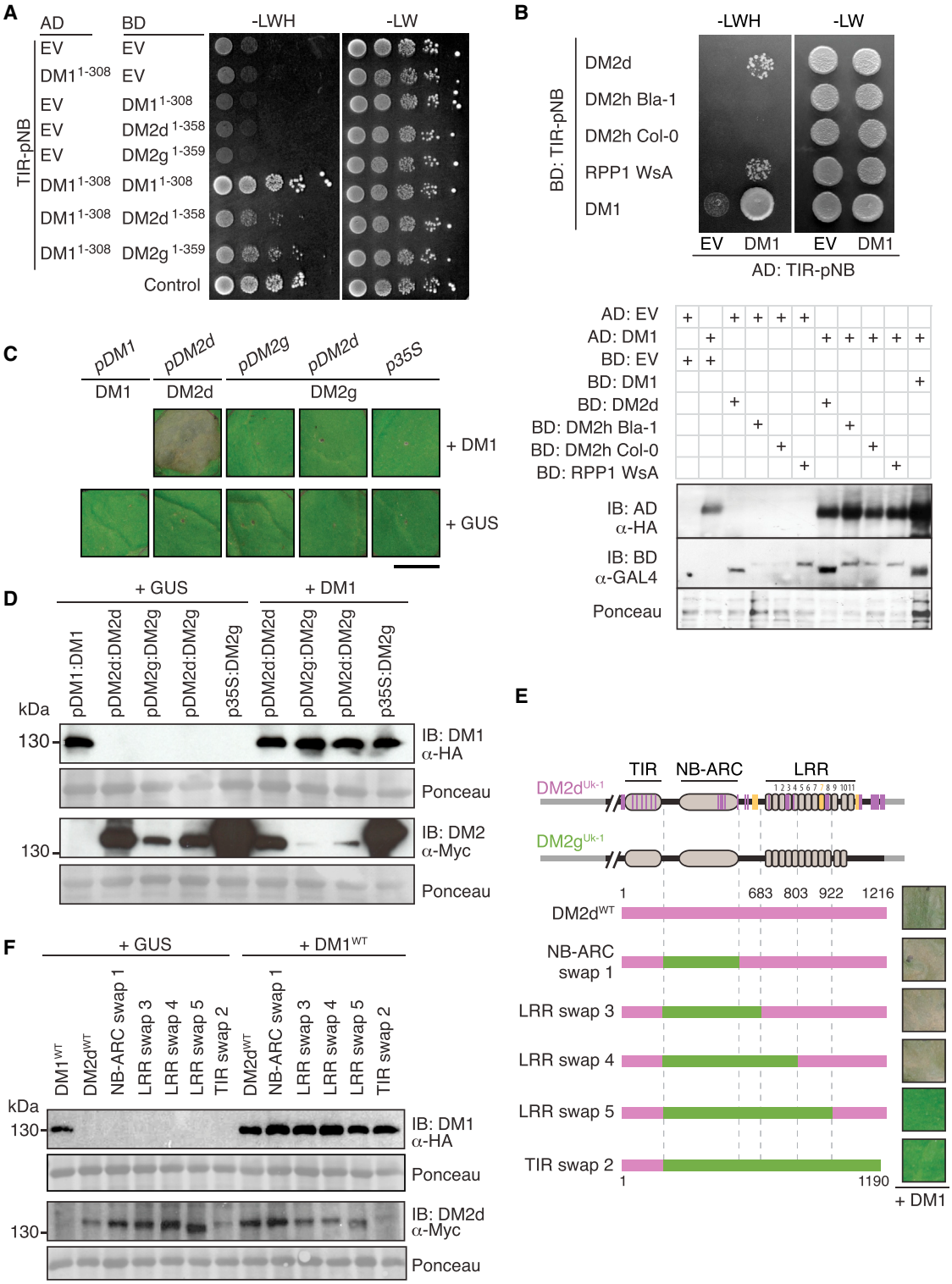

Figure 5. Association of DM1/DM2 Variants and Domains Determining DM2d Activity

(A) Y2H assays of the DM2g$^{1–359}$ TIR-pNB fragment. Similar to the homologous DM2d$^{1–358}$ fragment, it associates with DM1$^{1–308}$.

(B) Y2H assays of DM2h and RPP1 TIR-pNB fragments. RPP1 WsA, but not DM2h-type, variants interact with DM1$^{1–308}$. Protein blots show that all of the fragments were expressed in yeast. Note that DM2h-type variants have an extended N-terminal region before the TIR domain (N-TIR) similar to RPP1 WsB and NdA variants (Figure S5A) [7].

(C) Lack of HR in *N. benthamiana* by co-expression of DM1^{WT} and DM2g under different promoters (4 dpi). Scale bar, 1 cm.

(legend continued on next page)

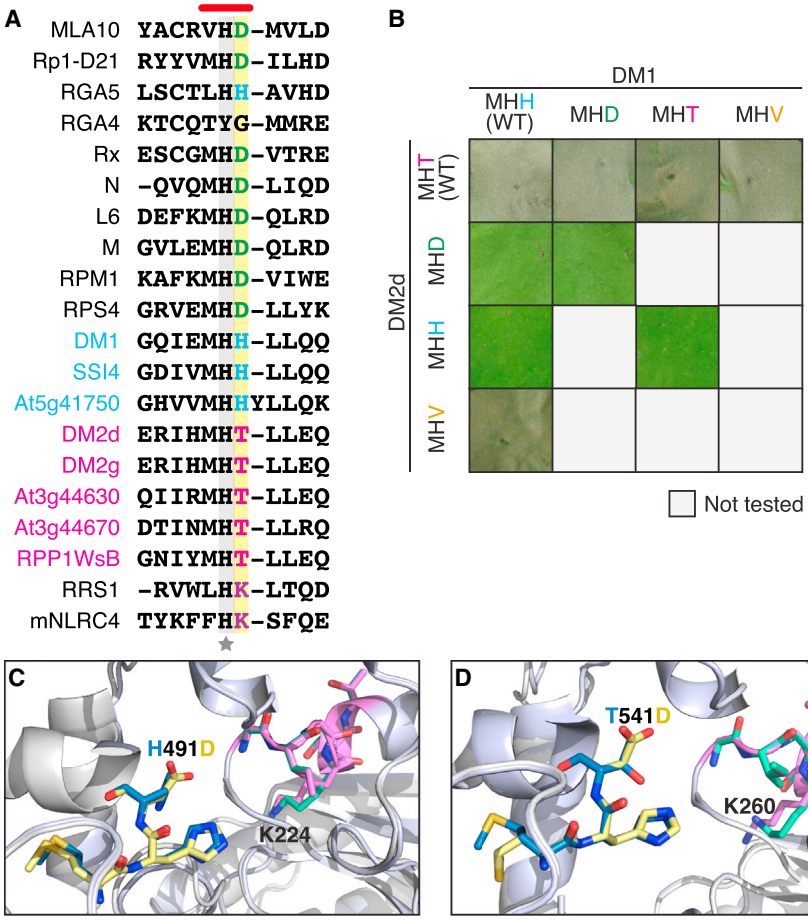

Figure 6. Effects of Mutations in MHD-like Motifs of DM1 and DM2d

(A) Sequence alignments of the MHD-like motif of plant NLRs and mouse NLRC4. The central histidine is invariant. A few plant proteins have an alternative residue in the first position. The third position is the one that is most variable. The star below the mNLRC4 sequence indicates a residue that causes autoimmunity when mutated [49]. DM1 homologs are labeled in cyan, and DM2 homologs are in magenta. The red bar indicates the location of the MHD motif.

(B) Summary of effects of mutations of MHD-like motifs on HR in *N. benthamiana* (4 dpi).

(C and D) Models of MHD-like motifs in DM1 (C) and DM2d (D) superimposed on the structure of mouse NLRC4 [49]. For wild-type proteins, P loops are highlighted in pink and MHD-like motifs are in blue. For mutated proteins, P loop motifs are highlighted in green and MHD-like motifs are in yellow. Nitrogen and oxygen atoms of amino acids are indicated in aqua blue and red. See also Figure S6.

DM2g (Figure 5E, LRR swaps 3, 4, and 5). The results with the first three chimeras pointed to LRRs 5–8 being important (Figures 5E and 5F). Additional chimeras showed, however, that these LRRs were not sufficient for activation (Figures S4D and S4F, LRR swaps 6, 7, and 8), indicating that differences in the second half of the LRR domain and the extended C-terminal region, which include several indels (Figure S5B), are critical. Together, we conclude that polymorphisms in the TIR domain, the second half of the LRR domain, and the extended C-terminal end of DM2d confer the ability to trigger autoimmunity through DM1, presumably by affecting intramolecular inhibitory interactions [7].

Unequal Contributions of DM1 and DM2d to Signaling

DM1 and DM2d and their paralogs have variant MHD motifs, MHH or MHT (Figure 6A). Non-canonical MHD-like motifs are also found in other plant NLRs, particularly in NLRs whose activity does not depend on a functional P loop, such as RRS1 and RGA5 (Figure 6A). To test the relevance of the third position of the MHD-like motif, we compared the activity of MHD, MHH, and MHV variants for DM1 and DM2d. When co-expressed with $DM2d^{WT}$, all mutated DM1 variants resulted in HR, whereas $DM2d^{T541D}$ and $DM2d^{T541H}$ did not (Figures 6B and S6A–S6D). Homology modeling based on mouse NLRC4 [49] (Figures S6E–S6J) suggested that T541D altered the orientation of the K260 amino tail in the P loop (Figure 6D) and that T541H changed the orientation of the histidine in the MHD-like motif (Figure S6I). The DM1 variants tested were not predicted to greatly alter arrangement of these residues (Figures 6C, S6G, and S6H). Given that both DM2d and DM2g exist in a heteromeric complex with DM1 but only DM1/DM2d is active (Figure 3F), we propose that the MHD-like motif, in concert with other polymorphisms (Figure 5E), confers a conformation on DM2d such that it is poised to trigger signaling upon interaction with DM1.

To further investigate the relative contribution of DM1 and DM2d to signaling, we designed a competition assay in which either partner is replaced with an increasing quantity of its inactive counterpart. We used transient expression in *N. benthamiana*, adding an *Agrobacterium tumefaciens* inoculum for the competitor at three different OD_{600}s (0.525, 1.05, and 2.1) to constant $DM1^{WT}$ and $DM2d^{WT}$ inocula (both at an OD_{600} of 0.525 before mixing).

(D) Protein blots for experiments shown in (C), with samples taken at 2 dpi.

(E) Domain swaps between DM2d and DM2g. Purple vertical lines indicate SNPs, and orange bars indicate indels. Green bars indicate DM2g fragments. The numbers refer to positions in DM2d. LRRs are numbered according to [36]. *N. benthamiana* leaves are shown on the right (4 dpi).

(F) Protein blots for experiments shown in (E), with samples taken at 2 dpi.

Ponceau-S staining is shown to indicate loading (B, D, and F).

See also Figures S4 and S5.

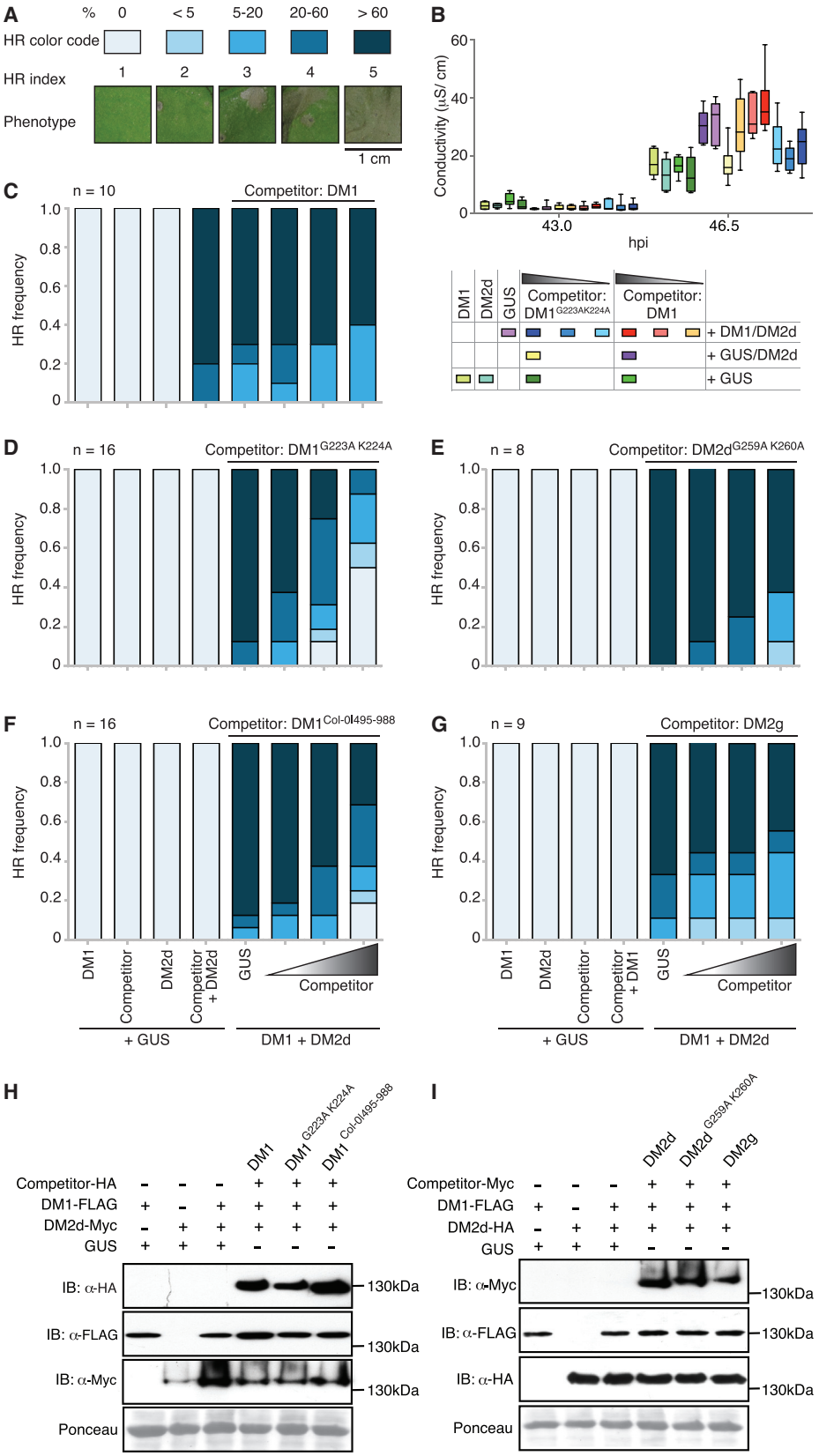

(legend on next page)

We first validated the competition assay system with $DM1^{WT}$ as competitor. Excess $DM1^{WT}$ did not change HR greatly (Figures 7A–7C and S7A), indicating that neither the increased inoculum nor the altered DM1:DM2d ratio affected our assay. We then tested as competitors two inactive DM1 variants, the P loop mutant ($DM1^{G223A\ K224A}$) (Figure 2C) and an inactive chimera carrying the LRR domain from innocuous At5g41750, the DM1 homolog from Col-0 ($DM1^{Col\text{-}0|495–988}$) (Figures S7B and S7C). Increasing amounts of either competitor reduced the HR extent, with $DM1^{G223A\ K224A}$ being a more effective competitor than $DM1^{Col\text{-}0|495–988}$ (Figures 7D, 7F, and 7H). Quantitative reduction in signaling by successive replacement of $DM1^{WT}$ with the inactive DM1 variants points to a critical signaling role of DM1 in the DM1/DM2 interaction.

Different from DM1, increasing amounts of DM2d competitors, the P loop mutant ($DM2d^{G259A\ K260A}$) (Figure 2D) or the close paralog DM2g (Figures 5C and S4B), were much less efficient in suppressing HR (Figures 7E, 7G, and 7I). Our interpretation of the limited effects of DM2d competitors is that small amounts of $DM2d^{WT}$ are sufficient to trigger immune signaling. We confirmed that the P loop mutants of DM1 and DM2d retained their interaction properties in Y2H assays, at least for the N-terminal interfaces (Figures S7D and S7E), arguing against changes in interaction properties being responsible for the failure of $DM2d^{G259A\ K260A}$ to compete with $DM2d^{WT}$.

DISCUSSION

We have described how two plant NLRs, DM1 and DM2d, interact to cause autoimmunity. The picture that emerges is that DM1 is the primary signal transducer, whereas DM2d triggers activation of a DM1 complex via heteromerization. Evidence for an unequal contribution of the two NLRs to signaling includes different effectiveness in competition assays and differential sensitivity to mutations that most likely affect protein conformation. Several characteristics differentiate the DM1/DM2d interaction from other heteromerizing plant NLRs. First, both DM1 and DM2d are required for signaling, which sets them apart from RGA4/RGA5 and RPS4/RRS1. In these cases, one protein alone, either full-length RGA4 or the RPS4 TIR domain, can trigger HR in *N. benthamiana*. Co-expression of the partner, either full-length RGA5 or the RRS1 TIR domain, suppresses autoimmunity [21, 22]. Second, the P loops need to be active in both DM1 and DM2d. In contrast, in the other two pairs, the P loop of the effector-binding NLR, RGA5 or RRS1, is dispensable [21, 22]. Third, the *DM1* and *DM2d* loci are unlinked in the genome, whereas *RGA4/RGA5* and *RPS4/RRS1* belong to a group of paired, divergently transcribed loci.

The DM1 and DM2d NLRs each forms a higher-order complex in the absence of signaling, with addition of DM2d altering the DM1 complex. We speculate that a pre-existing NLR complex may provide a scaffold for a particularly rapid immune response. In the mammalian inflammasome, the NLR NLRC4 acts as a scaffold. Although NLRC4 does not seem to have sensor function, gain-of-function mutations in an autoinhibitory helical domain can cause autoinflammatory disease [50]. In support of a signaling role of DM1, no cognate effector has so far been identified for *A. thaliana* DM1 homologs, but a gain-of-function mutation in a close paralog, *SSI4*, triggers autoimmunity [51]. A plausible hypothesis is that the DM1 complex transduces signals from other NLRs, presumably sensing non-self-triggered changes in the cell, via its affinity for TIR domains of other NLRs. We have demonstrated that the DM1 TIR domain can associate with the TIR domains of closely related DM2/RPP1 variants DM2d, DM2g, and RPP1 WsA but not with the N-TIR domains (Figure S5A) of two other RPP1 variants, $DM2h^{Col\text{-}0}$ and $DM2h^{Bla\text{-}1}$. This suggests the exciting possibility that DM1 supports signaling of other NLRs during pathogen-triggered immunity and that interaction properties of DM1 TIR determine which other TIRs can be signaling clients. Because Illumina read mapping indicates that *DM1*-like homologs are ubiquitous among *A. thaliana* accessions [52], it will be interesting to learn whether loss of *DM1* or a dominant-negative *DM1* variant affects effector triggered immunity (ETI) mediated by RPP1 variants with known cognate effectors.

The association of DM2 variants with DM1 suggests that NLR-NLR interactions occur more often than initially thought [53], presumably in an equilibrium status. Activation of the preformed complex would not merely depend on association with another NLR but on the activation potential of the other NLR, as shown by domain-swapping experiments using active DM2d and inactive DM2g. A major function of DM1 would thus be to provide a quantitative readout for conformation of another NLR, a concept similar to the proposed "helper" function of other plant NLRs [27–30]. Because in contrast to DM1, known helper NLRs do not require active P loops, we propose to classify DM1 as a "transducer" NLR.

How could a DM1 complex accommodate DM2d, with the TIR domain mediating both DM1-DM1 and DM1-DM2d association? We do not think that activation involves simple one-on-one competition for the same interaction interface. The DM1/DM2d complex might resemble the active NAIP2/NLRC4 inflammasome, in which the sensor NAIP2 and scaffolding NLRC4 are found in very different proportions [54]. NLRC4 apparently uses two different interfaces, one to bind to NAIP2 and the other to recruit additional NLRC4 molecules in a successive manner.

Figure 7. Suppression of DM1/DM2d Signaling by Inactive Competitors

(A) Semiquantitative scoring for HR in *N. benthamiana* for competition assays. Percentages indicate the fraction of HR in the field of view.

(B) Ion leakage as an indication of HR with a wild-type or P loop mutant DM1 competitor at 43 and 46.5 hpi. Boxes signify the upper and lower quartiles, and the median is represented by a horizontal black line within each box (n = 6).

(C–G) Competition assay with wild-type DM1 as a negative control (C), P loop mutant $DM1^{G223A\ K224A}$ (D), P loop mutant $DM2d^{G259A\ K260A}$ (E), inactive DM1 chimera $DM1^{Col\text{-}0|495–988}$ (F), or DM2g (G). Three different amounts of each competitor (OD_{600} = 0.525, 1.05, or 2.1) were mixed with constant amounts of wild-type DM1 and DM2d (both at OD_{600} = 0.525 before mixing). HR was scored at 4 dpi.

(H and I) Protein blots for competition assays with the highest amount of competitor (OD_{600} = 2.1) of DM1 (H) and of DM2d (I). Samples were taken at 40 hpi. Blots indicate no sign of co-suppression of the seed inoculum of DM1 and DM2d. Ponceau-S staining is shown to indicate loading.

See also Figure S7.

Our competition assays suggest that a small amount of DM2d can trigger signaling, implying uneven stoichiometry of DM1 and DM2d in the DM1/DM2d signaling complex. Different from NAIP2/NLRC4, DM1 presumably preforms a higher-order complex, possibly a tetramer (Figure 3F). Its signaling activity is switched on upon association with DM2d, but not with DM2g. Signaling could be initiated either by entry of DM2d into the complex, leading to recruitment of additional DM1 molecules to the complex, or by heteromeric DM2d association, filling a "gap" to complete complex formation. We also cannot exclude the possibility of de novo heteromeric complex formation. In either scenario, heteromeric interaction between DM1 and DM2d greatly facilitates full activation of the complex.

DM2d is encoded by a superlocus encoding multiple RPP1 homologs for which direct and specific association with cognate effectors has been demonstrated [14, 15]. Although RPP1 clearly has a "sensor" function and effector-triggered TIR self-association is required for signaling [7], it is not clear whether RPP1 signals alone or in combination with another NLR. Extensive analyses of the effector-binding NLRs RPP1 and L6 have suggested that the sensor domain co-evolves with other domains to generate multiple variants, each of which can occupy a distinct position in a gradual transition toward full NLR activity [13, 14]. Bernoux and colleagues have shown for the L6 and L7 NLRs that their different activation potentials correlate with ATP-dependent equilibrium status, which can be independent of effector binding [18]. An attractive hypothesis is that DM2d mimics a conformation that other DM2 variants only adopt upon effector recognition, with its peculiar conformation endowing DM2d with the ability to autonomously trigger immune responses through the DM1 complex. This hypothesis is supported by the finding that mutations predicted to change DM2d conformation (Figure S6) reduce signaling, whereas DM1 is much less sensitive to similar mutations (Figure 6). We also interpret the inactivity of the DM2d P loop mutant (Figure 2B) as being primarily due to conformational changes. Another *DM2* allele, *DM2h*^{Ler}, an ortholog of the *DM2h*$^{Bla-1}$ hybrid necrosis risk allele [36], triggers EDS1-dependent autoimmunity in combination with different second-site changes in the genome [55]. The extended C-terminal end makes a critical contribution to DM2h^{Ler} function, similar to what we found for DM2d (Figures 5E and S5B). If indeed the overall conformation is a major determinant of DM2-mediated autoimmune activity, either in combination with DM1 or with other molecules, this would support our assertion that specific DM2 variants, and by extension perhaps other members of the RPP1 locus, function as sensitized signaling switches.

The scenario of DM1 as transducer and DM2d as trigger does not imply that the two NLRs only function with each other. Instead, DM1 might be considered a facultative guard of sensor NLRs that easily change their conformation. If many NLRs utilize a conserved interaction interface [22], a preformed NLR complex would present a particularly versatile element in the immune response. Although many NLRs are most likely under diversifying selective pressure, the TIR and CC signaling domains are rather conserved and may provide a preformed hub for signal transduction. There are limited examples of interacting NLR pairs, and so far the field has focused on those that co-evolve because they are genetically tightly linked [56].

In summary, our work has shown that the study of hybrid necrosis can reveal new aspects of immune signaling in plants. An important question for the future is whether DM1, compared to its paralogs, has special properties that extend beyond differential interaction with DM2 paralogs and, if yes, what evolutionary forces are responsible for them.

EXPERIMENTAL PROCEDURES

Plant Material

Plants were grown in long days (16 hr light/8 hr dark). Table S1 lists stocks used for transformation with *DM1* and *DM2d* constructs. To induce the expression of *indDM1-HA* in 15-day-old *A. thaliana* plants, pots were irrigated with 1% ethanol and covered with a plastic dome for 72 hr. The same construct infiltrated in *N. benthamiana* was induced at 18 hr post-infiltration (hpi) by irrigation with 1% ethanol for 18 hr.

Transient Expression in *N. benthamiana*

A. tumefaciens was grown to an OD_{600} of 1.2–1.8, and then incubated in induction medium (10 mM MES [pH 5.6], 10 mM $MgCl_2$, and 150 μM acetosyringone). The cell suspensions were normalized to an OD_{600} of 0.35, and mixed 1:1 for co-infiltration into the abaxial side of *N. benthamiana* leaves. For competition assays, competitor OD_{600} was adjusted to 0.525, 1.05, and 2.1; OD_{600} for wild-type DM1 or DM2d was 0.525. HR was quantified by measuring ion leakage using an Orion Star conductivity meter (Thermo Scientific) in eight replicates.

Yeast Two-Hybrid Assay

See the Supplemental Experimental Procedures for details.

Protein Extraction and Co-immunoprecipitation Assay

For detection of DM1 and DM2 proteins in *N. benthamiana* and *A. thaliana*, microsomal fractions of the samples were prepared. Co-immunoprecipitation assays were performed using total protein extract from 500 mg of *N. benthamiana* or 1 g of *A. thaliana* leaf tissue. See the Supplemental Experimental Procedures for details.

Blue Native-PAGE

0.5 g of fresh leaf samples from 2-week-old seedlings was collected and ground in solubilization buffer (30 mM HEPES-KOH [pH 7.5], 150 mM potassium acetate, 10% [v/v] glycerol, 0.5% *n*-dodecyl β-maltoside, and 1× plant protease inhibitor cocktail), followed by centrifugation for 10 min at top speed. 20 μg of protein extract was mixed with 6 μL of 4× NativePAGE sample buffer and 0.06 μL of NativePAGE 5% G-250 Sample Additive (Invitrogen). 32 μL of total sample was loaded and run on a NativePAGE 3%–12% Bis-Tris gel for the primary dimension followed by incubation in 1% SDS for 15 min. Denatured gel strips were separated at constant polyacrylamide concentration (7.5%), as suggested by the supplier (Invitrogen). SDS-PAGE followed by immunoblot with anti-Myc or anti-HA was performed.

SUPPLEMENTAL INFORMATION

Supplemental Information includes Supplemental Experimental Procedures, seven figures, and one table and can be found with this article online at http://dx.doi.org/10.1016/j.cub.2017.03.018.

AUTHOR CONTRIBUTIONS

D.T.N.T., E.-H.C., R.S., J.L.D., D.W., and E.C. conceived, designed, and coordinated the research. D.T.N.T., E.-H.C., A.H.-M., M.D., and E.C. conducted the experiments. D.T.N.T., E.-H.C., and E.C. analyzed the data. D.T.N.T., J.L.D., D.W., and E.C. wrote the paper with help from all authors.

ACKNOWLEDGMENTS

We thank Kirsten Bomblies for the DM1$^{Col-0|495–988}$ construct, Iuliia Boichenko for advice on protein structure, Paula Sancha-Vilchez for technical support,

and Chang Liu, Gautam Shirsekar, Ignacio Rubio-Somoza, Adam Steinbrenner, and the Weigel laboratory for discussions. Funded by grants from the NSF (IOS-1257373) and the Gordon and Betty Moore Foundation (GBMF3030) (J.L.D.), HFSPO (RGP 57/2007) (J.L.D. and D.W.), ERC Advanced Grant IMMUNEMESIS (340602), and the Max Planck Society (D.W.). J.L.D. is an Investigator of the Howard Hughes Medical Institute, supported by the HHMI and a Distinguished Guest Professorship of the University of Tübingen.

Received: August 18, 2016
Revised: February 9, 2017
Accepted: March 9, 2017
Published: April 13, 2017

REFERENCES

1. Maekawa, T., Kufer, T.A., and Schulze-Lefert, P. (2011). NLR functions in plant and animal immune systems: so far and yet so close. Nat. Immunol. *12*, 817–826.
2. Dangl, J.L., and Jones, J.D. (2001). Plant pathogens and integrated defence responses to infection. Nature *411*, 826–833.
3. van der Hoorn, R.A., and Kamoun, S. (2008). From guard to decoy: a new model for perception of plant pathogen effectors. Plant Cell *20*, 2009–2017.
4. Sukarta, O.C., Slootweg, E.J., and Goverse, A. (2016). Structure-informed insights for NLR functioning in plant immunity. Semin. Cell Dev. Biol. *56*, 134–149.
5. Bernoux, M., Ve, T., Williams, S., Warren, C., Hatters, D., Valkov, E., Zhang, X., Ellis, J.G., Kobe, B., and Dodds, P.N. (2011). Structural and functional analysis of a plant resistance protein TIR domain reveals interfaces for self-association, signaling, and autoregulation. Cell Host Microbe *9*, 200–211.
6. Maekawa, T., Cheng, W., Spiridon, L.N., Töller, A., Lukasik, E., Saijo, Y., Liu, P., Shen, Q.H., Micluta, M.A., Somssich, I.E., et al. (2011). Coiled-coil domain-dependent homodimerization of intracellular barley immune receptors defines a minimal functional module for triggering cell death. Cell Host Microbe *9*, 187–199.
7. Schreiber, K.J., Bentham, A., Williams, S.J., Kobe, B., and Staskawicz, B.J. (2016). Multiple domain associations within the *Arabidopsis* immune receptor RPP1 regulate the activation of programmed cell death. PLoS Pathog. *12*, e1005769.
8. Mestre, P., and Baulcombe, D.C. (2006). Elicitor-mediated oligomerization of the tobacco N disease resistance protein. Plant Cell *18*, 491–501.
9. Cesari, S., Moore, J., Chen, C., Webb, D., Periyannan, S., Mago, R., Bernoux, M., Lagudah, E.S., and Dodds, P.N. (2016). Cytosolic activation of cell death and stem rust resistance by cereal MLA-family CC-NLR proteins. Proc. Natl. Acad. Sci. USA *113*, 10204–10209.
10. Casey, L.W., Lavrencic, P., Bentham, A.R., Cesari, S., Ericsson, D.J., Croll, T., Turk, D., Anderson, P.A., Mark, A.E., Dodds, P.N., et al. (2016). The CC domain structure from the wheat stem rust resistance protein Sr33 challenges paradigms for dimerization in plant NLR proteins. Proc. Natl. Acad. Sci. USA *45*, 12856–12861.
11. Botella, M.A., Parker, J.E., Frost, L.N., Bittner-Eddy, P.D., Beynon, J.L., Daniels, M.J., Holub, E.B., and Jones, J.D. (1998). Three genes of the *Arabidopsis RPP1* complex resistance locus recognize distinct *Peronospora parasitica* avirulence determinants. Plant Cell *10*, 1847–1860.
12. Dodds, P.N., Lawrence, G.J., Catanzariti, A.M., Teh, T., Wang, C.I., Ayliffe, M.A., Kobe, B., and Ellis, J.G. (2006). Direct protein interaction underlies gene-for-gene specificity and coevolution of the flax resistance genes and flax rust avirulence genes. Proc. Natl. Acad. Sci. USA *103*, 8888–8893.
13. Ravensdale, M., Bernoux, M., Ve, T., Kobe, B., Thrall, P.H., Ellis, J.G., and Dodds, P.N. (2012). Intramolecular interaction influences binding of the Flax L5 and L6 resistance proteins to their AvrL567 ligands. PLoS Pathog. *8*, e1003004.
14. Steinbrenner, A.D., Goritschnig, S., and Staskawicz, B.J. (2015). Recognition and activation domains contribute to allele-specific responses of an *Arabidopsis* NLR receptor to an oomycete effector protein. PLoS Pathog. *11*, e1004665.
15. Krasileva, K.V., Dahlbeck, D., and Staskawicz, B.J. (2010). Activation of an *Arabidopsis* resistance protein is specified by the in planta association of its leucine-rich repeat domain with the cognate oomycete effector. Plant Cell *22*, 2444–2458.
16. Stirnweis, D., Milani, S.D., Jordan, T., Keller, B., and Brunner, S. (2014). Substitutions of two amino acids in the nucleotide-binding site domain of a resistance protein enhance the hypersensitive response and enlarge the PM3F resistance spectrum in wheat. Mol. Plant Microbe Interact. *27*, 265–276.
17. Harris, C.J., Slootweg, E.J., Goverse, A., and Baulcombe, D.C. (2013). Stepwise artificial evolution of a plant disease resistance gene. Proc. Natl. Acad. Sci. USA *110*, 21189–21194.
18. Bernoux, M., Burdett, H., Williams, S.J., Zhang, X., Chen, C., Newell, K., Lawrence, G.J., Kobe, B., Ellis, J.G., Anderson, P.A., and Dodds, P.N. (2016). Comparative analysis of the flax immune receptors L6 and L7 suggests an equilibrium-based switch activation model. Plant Cell *28*, 146–159.
19. Slootweg, E.J., Spiridon, L.N., Roosien, J., Butterbach, P., Pomp, R., Westerhof, L., Wilbers, R., Bakker, E., Bakker, J., Petrescu, A.J., et al. (2013). Structural determinants at the interface of the ARC2 and leucine-rich repeat domains control the activation of the plant immune receptors Rx1 and Gpa2. Plant Physiol. *162*, 1510–1528.
20. Wang, G.F., Ji, J., El-Kasmi, F., Dangl, J.L., Johal, G., and Balint-Kurti, P.J. (2015). Molecular and functional analyses of a maize autoactive NB-LRR protein identify precise structural requirements for activity. PLoS Pathog. *11*, e1004674.
21. Césari, S., Kanzaki, H., Fujiwara, T., Bernoux, M., Chalvon, V., Kawano, Y., Shimamoto, K., Dodds, P., Terauchi, R., and Kroj, T. (2014). The NB-LRR proteins RGA4 and RGA5 interact functionally and physically to confer disease resistance. EMBO J. *33*, 1941–1959.
22. Williams, S.J., Sohn, K.H., Wan, L., Bernoux, M., Sarris, P.F., Segonzac, C., Ve, T., Ma, Y., Saucet, S.B., Ericsson, D.J., et al. (2014). Structural basis for assembly and function of a heterodimeric plant immune receptor. Science *344*, 299–303.
23. Sarris, P.F., Duxbury, Z., Huh, S.U., Ma, Y., Segonzac, C., Sklenar, J., Derbyshire, P., Cevik, V., Rallapalli, G., Saucet, S.B., et al. (2015). A plant immune receptor detects pathogen effectors that target WRKY transcription factors. Cell *161*, 1089–1100.
24. Le Roux, C., Huet, G., Jauneau, A., Camborde, L., Trémousaygue, D., Kraut, A., Zhou, B., Levaillant, M., Adachi, H., Yoshioka, H., et al. (2015). A receptor pair with an integrated decoy converts pathogen disabling of transcription factors to immunity. Cell *161*, 1074–1088.
25. Kofoed, E.M., and Vance, R.E. (2011). Innate immune recognition of bacterial ligands by NAIPs determines inflammasome specificity. Nature *477*, 592–595.
26. Zhao, Y., Yang, J., Shi, J., Gong, Y.N., Lu, Q., Xu, H., Liu, L., and Shao, F. (2011). The NLRC4 inflammasome receptors for bacterial flagellin and type III secretion apparatus. Nature *477*, 596–600.
27. Bonardi, V., Tang, S., Stallmann, A., Roberts, M., Cherkis, K., and Dangl, J.L. (2011). Expanded functions for a family of plant intracellular immune receptors beyond specific recognition of pathogen effectors. Proc. Natl. Acad. Sci. USA *108*, 16463–16468.
28. Peart, J.R., Mestre, P., Lu, R., Malcuit, I., and Baulcombe, D.C. (2005). NRG1, a CC-NB-LRR protein, together with N, a TIR-NB-LRR protein, mediates resistance against tobacco mosaic virus. Curr. Biol. *15*, 968–973.
29. Gabriëls, S.H., Vossen, J.H., Ekengren, S.K., van Ooijen, G., Abd-El-Haliem, A.M., van den Berg, G.C., Rainey, D.Y., Martin, G.B., Takken, F.L., de Wit, P.J., and Joosten, M.H. (2007). An NB-LRR protein required for HR signalling mediated by both extra- and intracellular resistance proteins. Plant J. *50*, 14–28.

30. Wu, C.H., Belhaj, K., Bozkurt, T.O., Birk, M.S., and Kamoun, S. (2016). Helper NLR proteins NRC2a/b and NRC3 but not NRC1 are required for Pto-mediated cell death and resistance in *Nicotiana benthamiana*. New Phytol. *209*, 1344–1352.
31. Bomblies, K., and Weigel, D. (2007). Hybrid necrosis: autoimmunity as a potential gene-flow barrier in plant species. Nat. Rev. Genet. *8*, 382–393.
32. Bomblies, K., Lempe, J., Epple, P., Warthmann, N., Lanz, C., Dangl, J.L., and Weigel, D. (2007). Autoimmune response as a mechanism for a Dobzhansky-Muller-type incompatibility syndrome in plants. PLoS Biol. *5*, e236.
33. Alcázar, R., von Reth, M., Bautor, J., Chae, E., Weigel, D., Koornneef, M., and Parker, J.E. (2014). Analysis of a plant complex resistance gene locus underlying immune-related hybrid incompatibility and its occurrence in nature. PLoS Genet. *10*, e1004848.
34. Alcázar, R., García, A.V., Kronholm, I., de Meaux, J., Koornneef, M., Parker, J.E., and Reymond, M. (2010). Natural variation at Strubbelig Receptor Kinase 3 drives immune-triggered incompatibilities between *Arabidopsis thaliana* accessions. Nat. Genet. *42*, 1135–1139.
35. Yamamoto, E., Takashi, T., Morinaka, Y., Lin, S., Wu, J., Matsumoto, T., Kitano, H., Matsuoka, M., and Ashikari, M. (2010). Gain of deleterious function causes an autoimmune response and Bateson-Dobzhansky-Muller incompatibility in rice. Mol. Genet. Genomics *283*, 305–315.
36. Chae, E., Bomblies, K., Kim, S.T., Karelina, D., Zaidem, M., Ossowski, S., Martín-Pizarro, C., Laitinen, R.A., Rowan, B.A., Tenenboim, H., et al. (2014). Species-wide genetic incompatibility analysis identifies immune genes as hot spots of deleterious epistasis. Cell *159*, 1341–1351.
37. Heidrich, K., Wirthmueller, L., Tasset, C., Pouzet, C., Deslandes, L., and Parker, J.E. (2011). *Arabidopsis* EDS1 connects pathogen effector recognition to cell compartment-specific immune responses. Science *334*, 1401–1404.
38. Bhattacharjee, S., Halane, M.K., Kim, S.H., and Gassmann, W. (2011). Pathogen effectors target *Arabidopsis* EDS1 and alter its interactions with immune regulators. Science *334*, 1405–1408.
39. Shirasu, K. (2009). The HSP90-SGT1 chaperone complex for NLR immune sensors. Annu. Rev. Plant Biol. *60*, 139–164.
40. Roberts, M., Tang, S., Stallmann, A., Dangl, J.L., and Bonardi, V. (2013). Genetic requirements for signaling from an autoactive plant NB-LRR intracellular innate immune receptor. PLoS Genet. *9*, e1003465.
41. Torres, M.A., Jones, J.D., and Dangl, J.L. (2005). Pathogen-induced, NADPH oxidase-derived reactive oxygen intermediates suppress spread of cell death in *Arabidopsis thaliana*. Nat. Genet. *37*, 1130–1134.
42. Swiderski, M.R., Birker, D., and Jones, J.D. (2009). The TIR domain of TIR-NB-LRR resistance proteins is a signaling domain involved in cell death induction. Mol. Plant Microbe Interact. *22*, 157–165.
43. Williams, S.J., Sornaraj, P., deCourcy-Ireland, E., Menz, R.I., Kobe, B., Ellis, J.G., Dodds, P.N., and Anderson, P.A. (2011). An autoactive mutant of the M flax rust resistance protein has a preference for binding ATP, whereas wild-type M protein binds ADP. Mol. Plant Microbe Interact. *24*, 897–906.
44. van Ooijen, G., Mayr, G., Kasiem, M.M., Albrecht, M., Cornelissen, B.J., and Takken, F.L. (2008). Structure-function analysis of the NB-ARC domain of plant disease resistance proteins. J. Exp. Bot. *59*, 1383–1397.
45. Tameling, W.I., Vossen, J.H., Albrecht, M., Lengauer, T., Berden, J.A., Haring, M.A., Cornelissen, B.J., and Takken, F.L. (2006). Mutations in the NB-ARC domain of I-2 that impair ATP hydrolysis cause autoactivation. Plant Physiol. *140*, 1233–1245.
46. Nishimura, M.T., Anderson, R.G., Cherkis, K.A., Law, T.F., Liu, Q.L., Machius, M., Nimchuk, Z.L., Yang, L., Chung, E.H., El Kasmi, F., et al. (2017). TIR-only protein RBA1 recognizes a pathogen effector to regulate cell death in *Arabidopsis*. Proc. Natl. Acad. Sci. USA *114*, E2053–E2062.
47. Zhang, X., Bernoux, M., Bentham, A.R., Newman, T.E., Ve, T., Casey, L.W., Raaymakers, T.M., Hu, J., Croll, T.I., Schreiber, K.J., et al. (2017). Multiple functional self-association interfaces in plant TIR domains. Proc. Natl. Acad. Sci. USA *114*, E2046–E2052.
48. Williams, S.J., Yin, L., Foley, G., Casey, L.W., Outram, M.A., Ericsson, D.J., Lu, J., Boden, M., Dry, I.B., and Kobe, B. (2016). Structure and function of the TIR domain from the grape NLR protein RPV1. Front. Plant Sci. *7*, 1850.
49. Hu, Z., Yan, C., Liu, P., Huang, Z., Ma, R., Zhang, C., Wang, R., Zhang, Y., Martinon, F., Miao, D., et al. (2013). Crystal structure of NLRC4 reveals its autoinhibition mechanism. Science *341*, 172–175.
50. Vance, R.E. (2015). The NAIP/NLRC4 inflammasomes. Curr. Opin. Immunol. *32*, 84–89.
51. Shirano, Y., Kachroo, P., Shah, J., and Klessig, D.F. (2002). A gain-of-function mutation in an *Arabidopsis* Toll Interleukin1 receptor-nucleotide binding site-leucine-rich repeat type R gene triggers defense responses and results in enhanced disease resistance. Plant Cell *14*, 3149–3162.
52. Cao, J., Schneeberger, K., Ossowski, S., Günther, T., Bender, S., Fitz, J., Koenig, D., Lanz, C., Stegle, O., Lippert, C., et al. (2011). Whole-genome sequencing of multiple *Arabidopsis thaliana* populations. Nat. Genet. *43*, 956–963.
53. Bonardi, V., and Dangl, J.L. (2012). How complex are intracellular immune receptor signaling complexes? Front. Plant Sci. *3*, 237.
54. Zhang, L., Chen, S., Ruan, J., Wu, J., Tong, A.B., Yin, Q., Li, Y., David, L., Lu, A., Wang, W.L., et al. (2015). Cryo-EM structure of the activated NAIP2-NLRC4 inflammasome reveals nucleated polymerization. Science *350*, 404–409.
55. Stuttmann, J., Peine, N., Garcia, A.V., Wagner, C., Choudhury, S.R., Wang, Y., James, G.V., Griebel, T., Alcázar, R., Tsuda, K., et al. (2016). *Arabidopsis thaliana DM2h (R8)* within the Landsberg *RPP1-like Resistance* locus underlies three different cases of *EDS1*-conditioned autoimmunity. PLoS Genet. *12*, e1005990.
56. Cesari, S., Bernoux, M., Moncuquet, P., Kroj, T., and Dodds, P.N. (2014). A novel conserved mechanism for plant NLR protein pairs: the "integrated decoy" hypothesis. Front. Plant Sci. *5*, 606.

Current Biology, Volume *27*

Supplemental Information

Activation of a Plant NLR Complex through Heteromeric Association with an Autoimmune Risk Variant of Another NLR

Diep T.N. Tran, Eui-Hwan Chung, Anette Habring-Müller, Monika Demar, Rebecca Schwab, Jeffery L. Dangl, Detlef Weigel, and Eunyoung Chae

Supplemental Figures

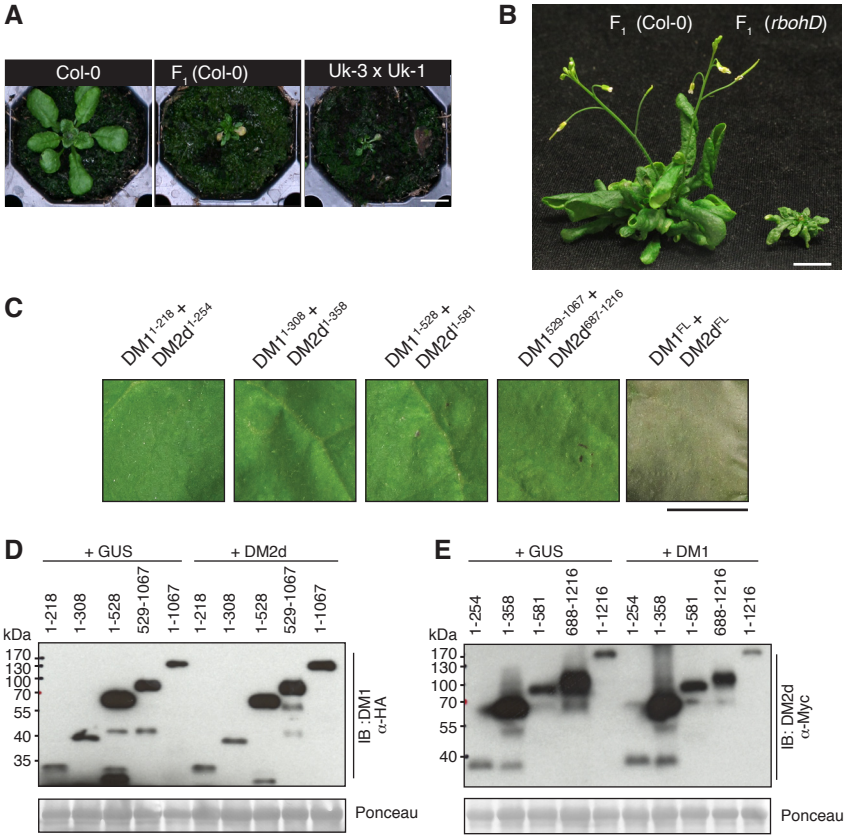

Figure S1. Recapitulation of hybrid necrosis in transgenic *A. thaliana*. Related to Figure 1

(A) Comparison of 30-day old F_1 hybrid for *gDM1-HA* x *gDM2d-Myc* in Col-0 wild-type background (middle) and Uk-3 x Uk-1 hybrid (right) [S1] grown at 16°C. Scale bar equals 1 cm.

(B) 55-day old *gDM1-HA* x *gDM2d-Myc* F_1 hybrids in Col-0 wild-type (left) and *rbohD* mutant (right) backgrounds grown at 16°C. The F_1 hybrid in Col-0 background eventually flowered and set seeds, but the one in *rbohD* background did not. Scale bar equals 1 cm.

(C) Representative effects of DM1/DM2d combinations (see Supplemental Experimental Procedures for construct information) in *N. benthamiana* at 4 dpi. Positional information is in Figure 2A-B. Scale bar equals 1 cm.

(D-E) Protein blots for experiments shown in (C), with samples taken at 2 dpi. Ponceau-S staining shown to indicate loading.

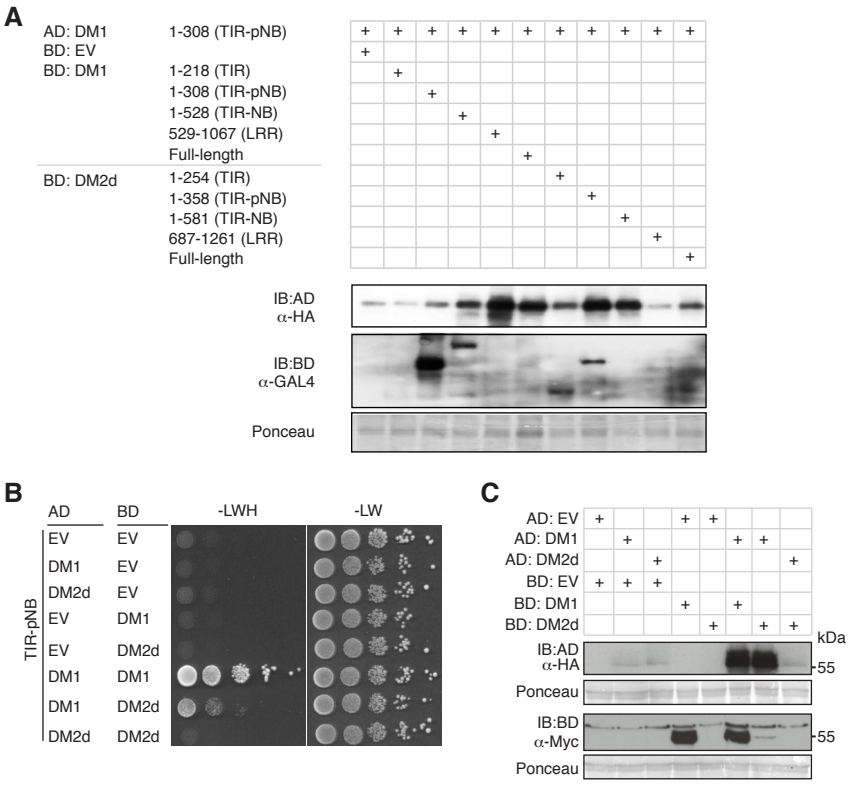

Figure S2. Y2H assay of DM1 and DM2d TIR-pNB fragments. Related to Figure 3

(A) Protein blot of samples shown in Figure 3A. TIR-pNB fragments of both DM1 and DM2d were well expressed, validating the usage of the fragments for further Y2H analyses. Neither LRR nor full-length proteins of DM1 and DM2d were detected. Despite non-detectable levels of TIR and full-length of DM1, Y2H interactions were positive.
AD: GAL4 activation domain, BD: GAL4 DNA-binding domain, EV: empty vector.
(B) Y2H analysis of DM1 and DM2d TIR-pNB fragments.
(C) Protein blot of samples shown in (B). DM2d TIR-pNB fused to BD was not detectable when DM1 TIR-pNB was not present.
Ponceau-S staining shown to indicate loading in (A) and (C).

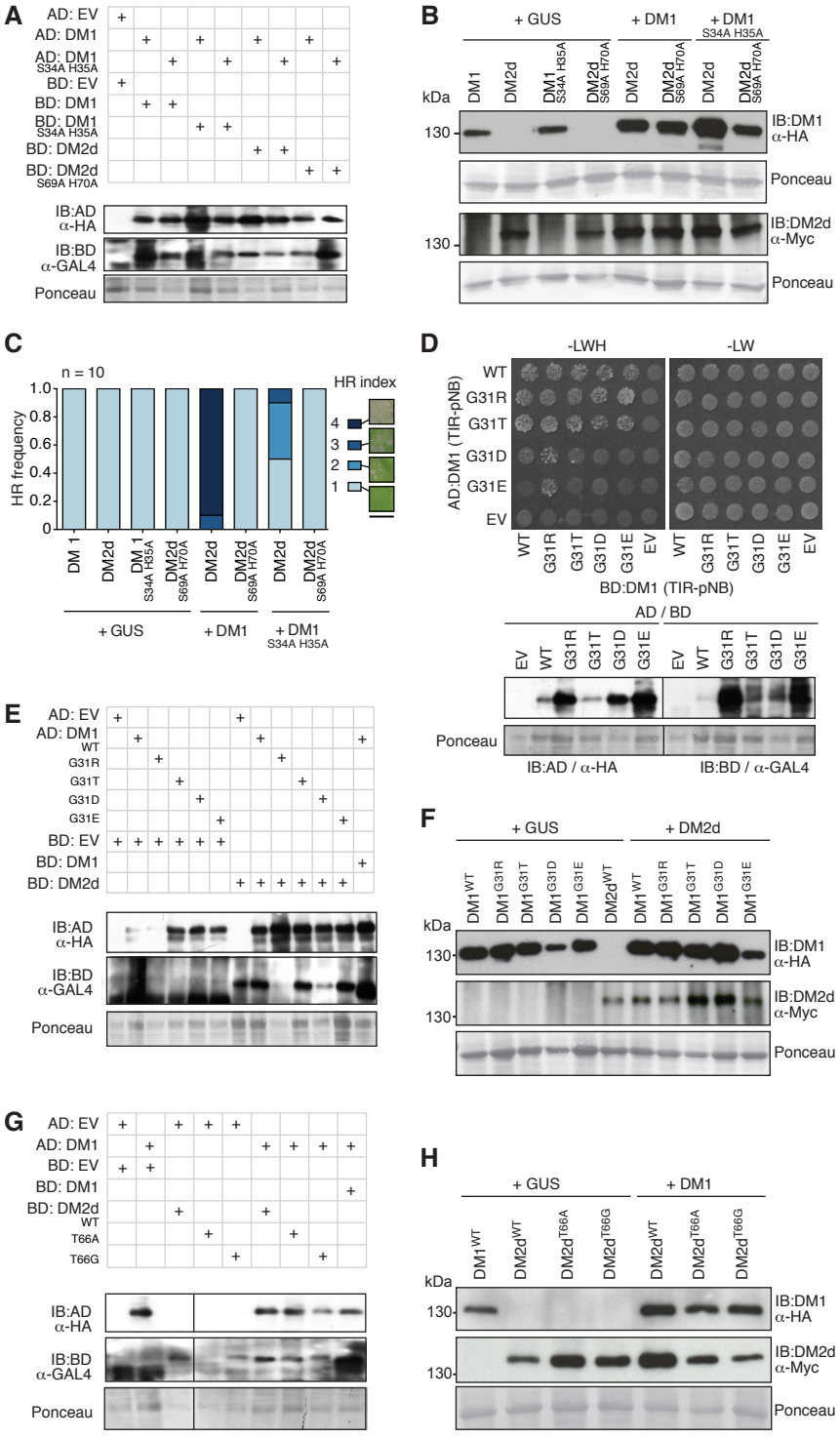

Figure S3. Characterization of DM1 and DM2d SH-motif mutants. Related to Figure 4

(A, E, G) Protein blots for Y2H shown in Figures 4A, 4C and 4E, respectively. All the DM1 and DM2d variants were expressed in yeast cells. AD fused proteins visualized with anti-HA blots and BD fused proteins with anti-GAL4 (DBD) blots.
(B, F, H) Protein blots for experiments shown in Figures 4B, 4D and 4F, respectively. All the DM1 and DM2d variants were expressed in *N. benthamiana*. Samples were taken at 2 dpi.

(C) Semi-quantitative scoring for HR in *N. benthamiana*. The HR index represents a percentage of area exhibiting HR in the infiltrated area as shown in the examples on the right at 4 dpi: 1 (no HR in field of view), 2 (less than 20% HR), 3 (20 to 60% HR) and 4 (over 60% HR). Scale bar equals 1 cm.
(D) Y2H assays with DM1 TIR-pNB fragments having different G31 substitutions and protein blots from the yeast cells carrying indicated constructs.
Ponceau-S staining shown to indicate loading (A, B, D-H)

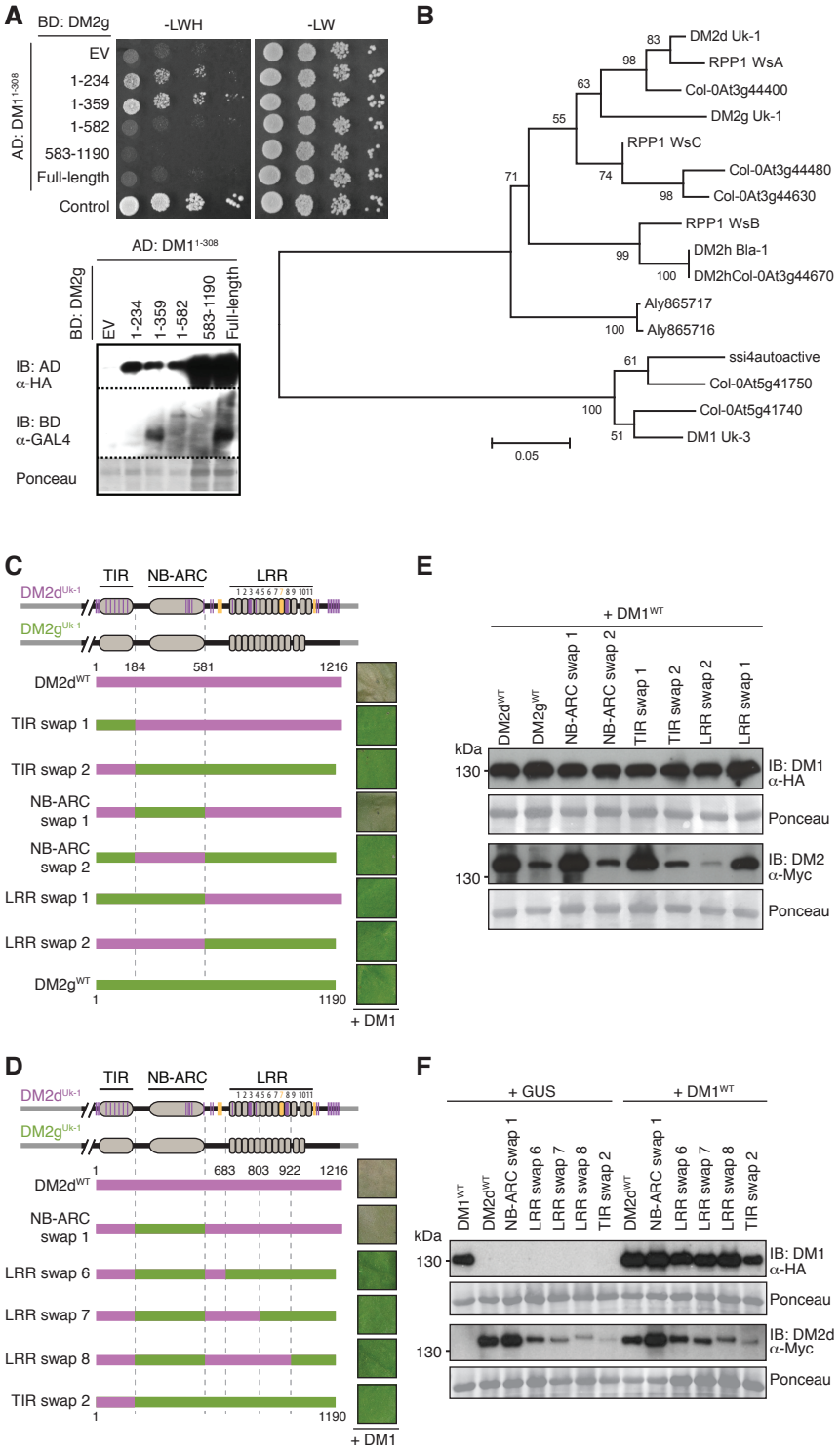

Figure S4. Domain swapping to localize functional differences between DM2d and DM2g. Related to Figure 5

(A) Y2H assay using DM1 TIR-pNB and DM2g fragments; the interaction is similar to that between DM1 and DM2d (see Figure 3A). Protein blots show LRR (583-1190) and full-length of DM2g are not detectable.

(B) Phylogeny constructed from amino acid sequences of TIR domains of DM2/RPP1 and DM1 proteins, using the Neighbor-Joining method based on the Kimura 2-parameter model implemented in MEGA5.
(C-D) Domain swaps between DM2d and DM2g. Purple vertical lines indicate SNPs and orange bars indels. Green bars indicate DM2g fragments. The numbers refer to positions in DM2d. *N. benthamiana* leaves are shown on right (4 dpi).
(E-F) Protein blots for experiments shown in Figures S4C and S4D, with samples collected 2 dpi. Ponceau-S staining shown to indicate loading.

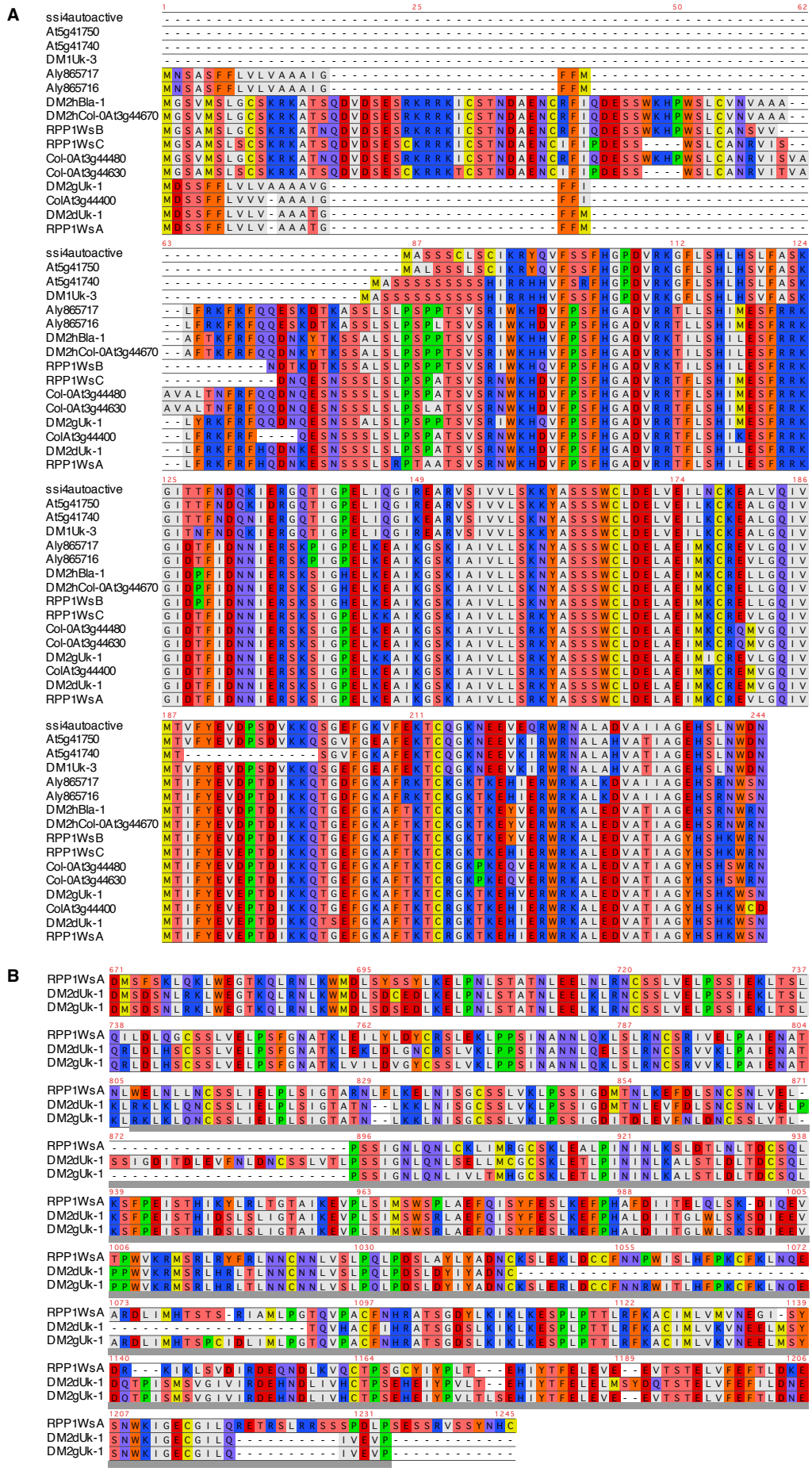
A
ssi4autoactive
At5g41750
At5g41740
DM1Uk-3
Aly865717
Aly865716
DM2hBla-1
DM2hCol-0At3g44670
RPP1WsB
RPP1WsC
Col-0At3g44480
Col-0At3g44630
DM2gUk-1
ColAt3g44400
DM2dUk-1
RPP1WsA
B
RPP1WsA
DM2dUk-1
DM2gUk-1

Figure S5. Amino acid alignment of TIR domain and LRR domain from multiple alleles of DM2/RPP1. Related to Figure 5

(A) Amino acid alignment of the N-terminal region sequences of DM1 and DM2/RPP1 alleles. DM2h types, RPP1 WsB/WsC, and their homologs from Col-0 (At3g44630, At3g44480) have the extended N-terminus, which was referred to N-TIR by [S2].
(B) Amino acid alignment of the C-terminal region sequences of DM2d/g and RPP1WsA, including LRR domains. Differences between DM2d and DM2g in the functionally critical region defined by domain swaps (underlined with gray bars) are mostly located close to indels: six polymorphisms in the duplicated LRR7 region in DM2d (853, 855, 860, 862, 866, 869), four (905, 906, 908, 910) C-terminal to the LRR7 duplication, two (1095, 1099) after the large indel (1045-1091), and small indels (1176-1177 and 1189-1190, 1192) at the extended C-terminus.

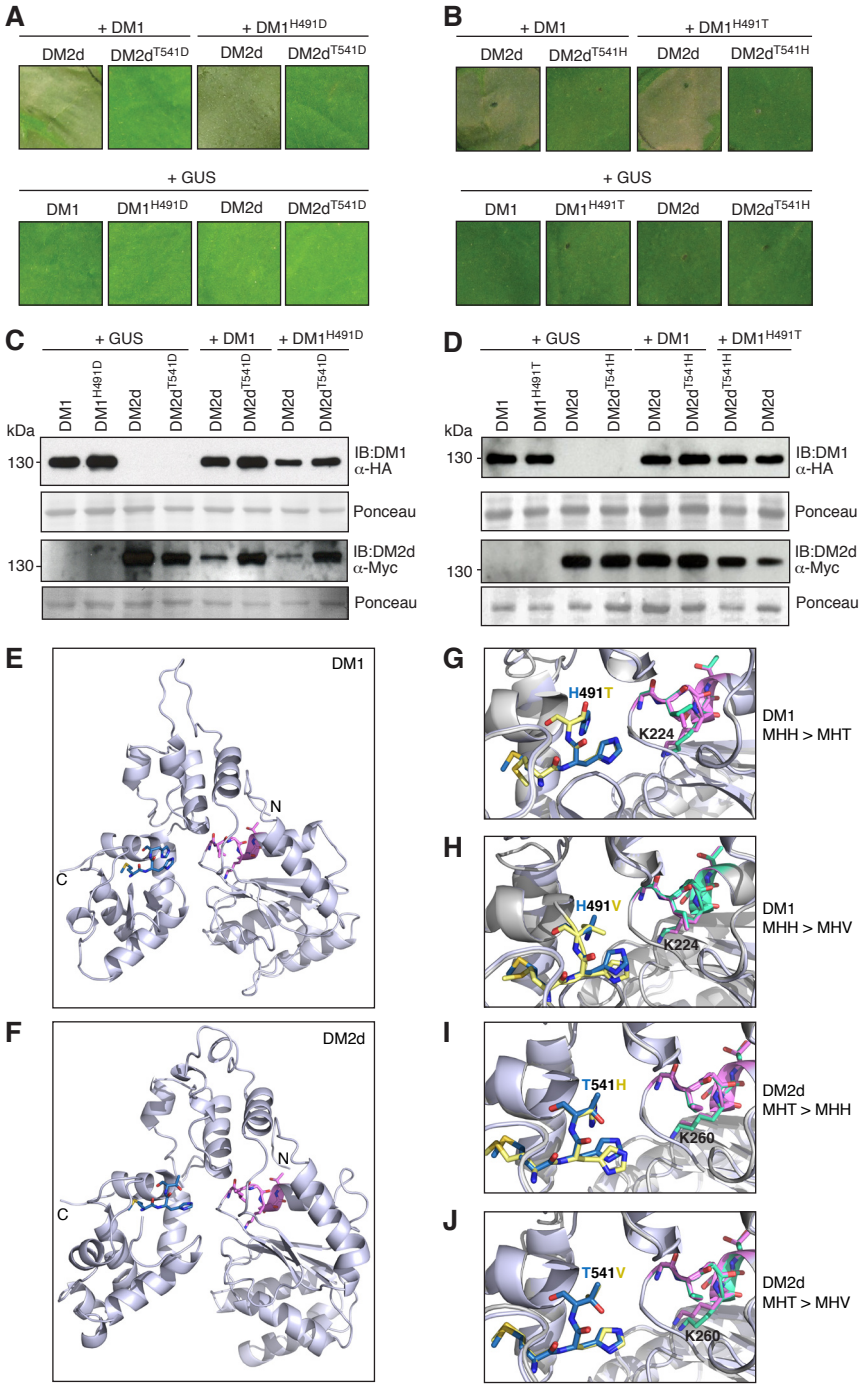

Figure S6. Additional characterization of DM1 and DM2d MHD-like motifs. Related to Figure 6

(A, B) DM1^{H491D}, DM1^{H491T}, DM2d^{T541H} and DM2d^{T541D} mutants were transiently co-expressed in *N. benthamiana* with the indicated partners. DM1^{H491D} and DM1^{H491T} functioned similar to the wild-type version, but DM2d^{T541D} and DM2d^{T541H} did not. HR phenotypes were scored at 4 dpi.

(C-D) Protein blots for experiments shown in (A, B), with samples taken 2 dpi. Ponceau-S staining shown to indicate loading.

(E-F) Homology modeling of NB-ARC domains of DM1 (E) and DM2d (F) based on that of mNLRC4 [S3] using the PHYRE2 web application [S4]. The P-loop and MHD-like motifs are highlighted in pink and blue.
(G-J) Superimposed models of MHD-like motifs in wild type and mutants. For wild-type proteins, P-loop motifs highlighted in pink and MHD-like motifs in blue. For mutated proteins, P-loops highlighted in green and MHD-like motifs in yellow.

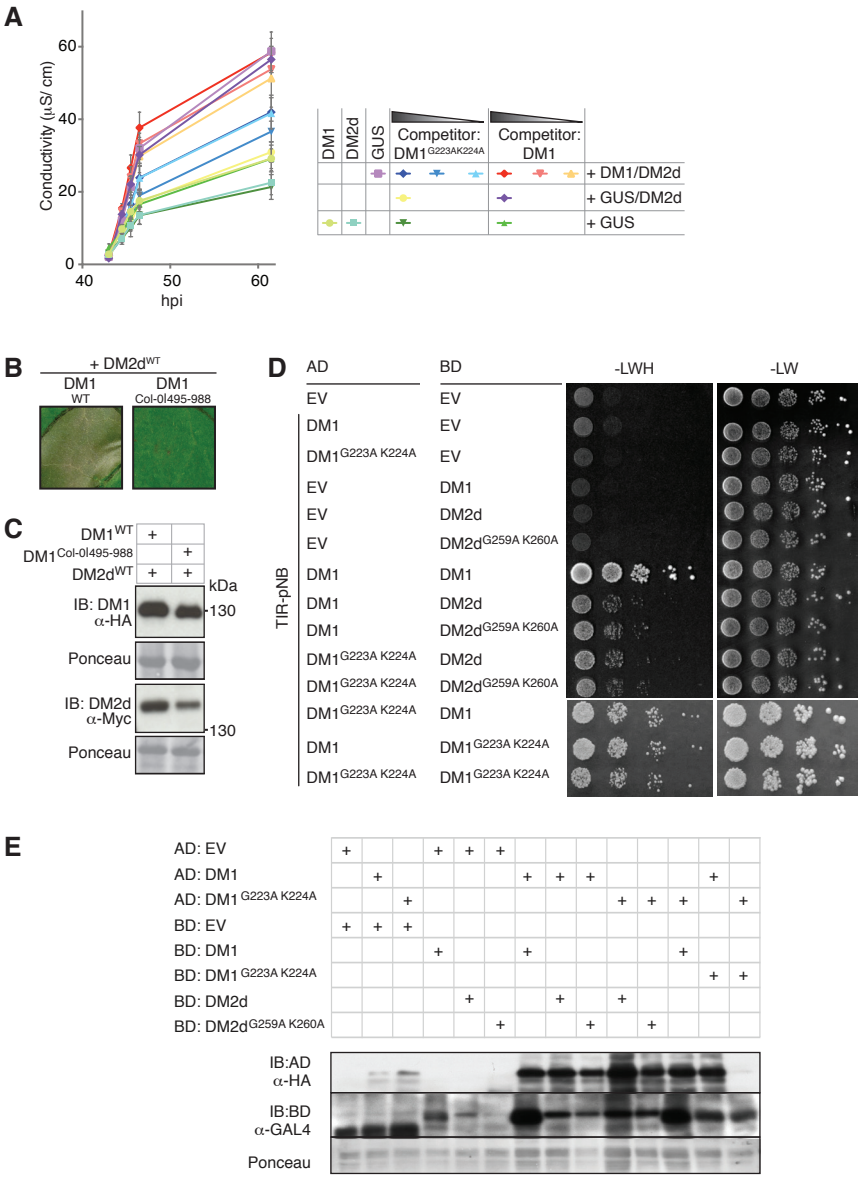

Figure S7. Additional characterization of DM1 and DM2 variants used in competition assays. Related to Figure 7

(A) Ion leakage as an indication of HR with wild-type or P-loop mutant DM1 competitor. Values are means ± SEM (n=6). hpi, hours post-infiltration

(B) HR at 4 dpi triggered by coexpression of DM1, but not DM1$^{Col\text{-}0|495\text{-}988}$ with DM2d in *N. benthamiana*. Scale bar equals 1 cm.

(C) Protein blots for experiment in (B), with samples taken at 2 dpi. Ponceau-S staining shown to indicate loading.

(D) Y2H analysis of TIR-pNB fragments of DM1 and DM2d carrying P-loop mutations. Both mutants behave like their wild-type counterparts.

(E) Protein blots for Y2H shown in (D). All the P-loop mutants were expressed comparable to their wild-type counterparts. Ponceau-S staining shown to indicate loading.

Supplemental Table

Table S1. Mutants used. Related to Figure 1

Mutant	Accession	Reference	Means of validation
eds1-1	Ws-0	[S5]	Sanger sequencing of PCR product
rar1-21	Col-0	[S6]	Sanger sequencing of PCR product
sgt1b	Col-0	[S7]	Sanger sequencing of PCR product
rbohD (SALK_074825)	Col-0	[S8]	Size of PCR product across T-DNA insertion site

Supplemental Experimental Procedures

Plant Transformation

A. thaliana seeds were surface sterilized with 70% ethanol solution with 0.5% (v/v) Triton X-100 before sowing. Plants were grown in a walk-in growth chamber with 125 to 175 µmol m^{-2} s^{-1} light intensity, 16 hour light/ 8 hour dark, 65% humidity. *A. thaliana* plants were transformed using the floral dip method [S9]. Transgenic lines carrying one copy of either *gDM1-2xHA* (pEC209), *gDM2d-4xMyc* (pMD325), or *indDM1-HA* (pDT010) in Col-0 wild-type or mutant backgrounds were identified on soil treated with 0.183 g/l Basta (glufosinate) and further bred to homozygosity in T_3. The F_1 hybrids used in this study were generated by crossing T_3 homozygous lines carrying each construct. Multiple independent lines were crossed to ensure robustness of results.

The F_1 hybrids of *indDM1-HA* and *gDM2d-4xMyc* were grown at 23°C on Basta treated soil. Expression of *DM1-HA* was induced in 15-days-old seedlings by irrigation with 1% ethanol. Ethanol treatment was performed by one-time irrigation and plants were covered by a plastic dome for 72 h. When domes were removed, remaining liquid in the tray was discarded. Necrosis was scored 3 days after ethanol treatment. Leaf sampling for co-immunoprecipitation was done 18 days after ethanol treatment.

Molecular Cloning

Site-directed mutagenesis was carried out by introducing corresponding changes in the primers and overlapping PCR. Genomic constructs of *DM1*, *DM2d* and *DM2g* and of their mutant derivatives were cloned to binary vectors by using conventional restriction enzymes or Gateway LR Cloning Technology (Invitrogen, Carlsbad, CA, USA). Primary sequences of the genic regions in all binary clones were confirmed with Sanger sequencing. Overlapping PCR method was used to generate all chimeric constructs, except for the NB-ARC domain swap constructs of DM2d/g. Six codon changes between DM2d and DM2g were introduced by site-directed mutagenesis in these chimeras. All the constructs with information on binary vector origins and primers used for overlapping PCR are listed at the end of this section.

The binary constructs were transformed into *A. tumefaciens* strain ASE by electroporation and transformants were selected on 25 µg/mL kanamycin, 25 µg/mL chloramphenicol, 100 µg/mL spectinomycin (for pGWB or pZZ006 constructs), or with the three antibiotics plus 25 µg/mL tetracycline (for pGREEN-IIS with pSOUP helper plasmid) [S10-S12]. Presence of plasmids was confirmed by colony PCR.

Expression Analyses

Total RNA from leaves of 20 day-old plants was extracted using acidified phenol [S13]. 1 µg of total RNA was used for cDNA synthesis using RevertAid RT Kit (Thermo Scientific, Vilnius, Lithuania) according to the manufacturer's protocol. cDNA was synthesized from 1 µg of total RNA using the RevertAid RT Kit (Thermo Scientific, Vilnius, Lithuania). The experiment was conducted with three independent F_1 lines and their parents and three technical replicates for each line.

Oligonucleotide primers for quantitative real-time PCR of *PR1*, *NPR1*, *WRKY46*, and *TUB2* control are listed at the end of this section. A PCR reaction mix, consisting of 2 µL of 1:5 diluted cDNA template, 0.25 µL of each primer at 100 pM, and 5 µL of Maxima SYBR Green Mix (Invitrogen, Carlsbad, CA, USA) in a total volume of 10 µL was prepared in three technical replicates. Relative expression of each target gene was measured by normalizing

CT value of the target gene to that of *TUB2* (ΔCT). To quantify the relative expression of the target gene in F_1 generation of *gDM1-2xHA* x *gDM2d-4xMyc* in wild type, and mutants (*eds1-1*, *rar1-21*, *sgt1b* and *rbohD*), ΔCT, value of the target gene in F_1 was calibrated to that of one of the parents carrying only *gDM1-2xHA* (ΔΔCT). The experiment was carried out with three independent lines of F_1 and parents. Each dot in Figure 1B represents –(ΔΔCT) value from a technical replicate, and data points from a biological replicate are marked with same color.

Transient Expression and Conductivity Assay

N. benthamiana plants were grown at 23°C and four to five week-old plants were used for *Agrobacterium tumefaciens*-mediated transient expression. *A. tumefaciens* (strain ASE) carrying a binary construct was grown overnight at 28°C in an orbital shaker at 200 rpm/min in 50 mL of LB medium containing appropriate antibiotics to OD_{600} of 1.2 to 1.8. Bacterial cells were harvested and resuspended in the induction medium containing 10 mM MES pH 5.6, 10 mM $MgCl_2$ and 150 µM acetosyringone with adjusted OD_{600} of 0.35. For *indDM1-HA* (pDT010), OD_{600} of 0.13 was used. After two hours of incubation in induction media at 28°C with 200 rpm/min, two bacterial inocula were mixed at 1:1 volume ratio with the addition of 1/10 volume of *Agrobacteria* carrying P19 to suppress transgene silencing. Bacterial mixtures were manually infiltrated using a 1-mL needleless syringe.

Expression of *indDM1-HA* was induced at 18 hpi by irrigating plants with 1% ethanol. Treated plants were kept under a plastic dome for additional 18 hours. At 36 hpi, five leaf discs (each with a diameter of 8 mm) from each plant were collected and floated in 15 mL water for 30 min. The leaf discs were transferred into a 6 ml tube with fresh water. Conductivity of samples in each tube was measured (µS/cm) using an Orion Star™ Conductivity Meter (Thermo Scientific, Beverly, MA, USA), from 36.75 to 60.75 hpi for seven to nine time points. The assay was carried out in eight biological replicates (5 discs x 8 plants) per indicated combination, and was repeated twice. One representative dataset is presented in Figure 2. Statistical analysis was carried out using GraphPad Prism v6.0c.

For competition assays, increasing amounts of the competitor inoculum (*A. tumefaciens* transformed with DT100, DT182, MD365 or MD366) were co-infiltrated with a premixed aliquot of DM1- and DM2d-expression constructs (EC209 and MD325). Before mixing, OD_{600} of each competitor was 0.525, 1.05 and 2.1, and of DM1 and DM2d were 0.525. Conductivity was measured from 43 hpi onward at five time points.

Yeast Two-Hybrid Assay

The Matchmaker GAL4 Two-Hybrid Systems (Clontech, Mountain View, CA, USA) was used with *Saccharomyces cerevisiae* strain AH109. Growth assays on minimal yeast media used 1:10 serial dilutions starting with OD_{600} of 0.5. At least four individual clones were used per assay and two independent assays were performed.

Yeast cells, grown from a colony in YPD medium at 30°C overnight, were harvested by centrifugation and lysed by a repetitive freezing and thawing for two minutes each. The crude protein extract was resuspended in 50 µL of 3X urea Laemmli buffer (240 mM Tris-HCl pH 6.8, 6% SDS, 30% glycerol, 16% β-mercaptoethanol, 0.006% bromophenol blue, 10 M Urea), denatured by boiling for 15 minutes, separated on 10% SDS-PAGE gel and immunoblotted on PVDF membrane (Bio-Rad, Foster City, CA, USA). AD- or BD-binding proteins were detected by anti-HA-peroxidase (Roche, Mannheim, Germany) (1:5,000 dilution), anti-c-Myc-horseradish peroxidase (HRP) (Sigma-Aldrich, Saint Louis, MO, USA) (1:15,000 dilution) or anti-GAL4 (DBD) (Santa Cruz Biotechnology, Dallas, TX, USA)

(1:1,000 dilution). Information on the control Y2H interaction (AD:RGL3 and BD:AP1) can be found [S14]**.**

Protein Expression in Plants

Microsomal fractions of the samples were prepared according to the reported method [S15] with the following modification. 100 mg leaf tissue was ground into fine powder in liquid nitrogen and homogenized in 210 µL of lysis buffer (0.33 M sucrose, 20 mM Tris-HCl pH 7.5, 1 mM EDTA, 10 mM DTT and 1 x cOmplete ULTRA Tablets, Mini, EDTA-free protease inhibitor cocktail (Roche). The lysate was cleared by a table-top centrifugation at 5,000 x g for 10 min at 4°C, and microsomal pellet fractions were collected by centrifugation at 20,000 g for 1 h at 4°C. Extracted proteins were resuspended in 2 x Laemmli sample buffer, boiled for 10 min at 95°C, separated on 7% SDS-PAGE gel and immunoblotted on PVDF membrane. The membrane was incubated with anti-c-Myc-HRP (Sigma-Aldrich) (1:15,000 dilution), or anti-HA-peroxidase (Roche) (1:5,000 dilution).

For co-immunoprecipitation assays, 500 mg of *N. benthamiana* or 1 g of *A. thaliana* leaf tissue was ground into fine powder in liquid nitrogen, and homogenized in 1 mL of extraction buffer (50 mM HEPES-KOH pH 7.5, 50 mM NaCl, 10 mM EDTA pH 8.0, 10 mM $MgCl_2$, 0.5% Tween-20, 5 mM DTT, 1x cOmplete ULTRA Tablets, Mini, EDTA-free protease inhibitor cocktail). The lysates were cleared by centrifugation at 10,000 g for 10 min at 4°C. 25 µL of Pierce™ anti-c-Myc magnetic beads or Pierce™ anti-HA magnetic beads (Thermo Scientific, Rockford, IL, USA) after equilibrating in the extraction buffer were mixed with the supernatants. After incubation for 4 hours at 4°C, the magnetic beads were collected and washed 3 times with washing buffer (same to the extraction buffer but containing 0.2% Tween-20). Bound proteins were collected by adding 50 µL of pre-heated elution buffer (50 mM Tris-HCl pH 6.8, 50 mM DTT, 1% SDS, 1 mM EDTA pH 8.0, 0.005% bromophenol blue, 10% glycerol). The immunoprecipitated proteins from anti-c-Myc were loaded on a 7% SDS-PAGE gel and detected after blotting with anti-c-Myc HRP (Sigma-Aldrich) (1:15,000 dilution) and anti-HA-peroxidase (Roche) (1:5,000 dilution).

BN-PAGE that we used to monitor DM1 and/or DM2d/g-containing protein complexes in *A. thaliana* essentially followed the protocol described in [S16]. The relative molecular weights of protein complexes were determined by loading 5 µl of NativeMark unstained protein ladder (ThermoFischer, Madison, WI. USA).

Binary T-DNA Constructs

Construct	Backbone	Promoter	Coding region
pDT010	pZZ006*	*palcA*	*DM1-2xHA*
pDT077	pGREENIIS	*pDM2d*	*TIR(DM2d)-NB(DM2g)-LRR(DM2d)-4xMyc*
pDT081	pGREENIIS	*pDM2d*	*TIR(DM2g)-NB(DM2d)-LRR(DM2d)-4xMyc*
pDT092	pGREENIIS	*p35S*	*DM2g-4xMyc*
pDT100	pGREENIIS	*pDM2d*	*DM2g-4xMyc*
pDT101	pGREENIIS	*pDM2d*	*TIR(DM2g)-NB(DM2d)-LRR(DM2g)-4xMyc*
pDT103	pGREENIIS	*pDM2d*	*TIR(DM2d)-NB(DM2g)-LRR(DM2g)-4xMyc*
pDT105	pGREENIIS	*pDM2d*	*DM2d$^{1-581}$-4xMyc*
pDT134	pGREENIIS	*pDM1*	*DM1^{H491V}-2xHA*
pDT135	pGREENIIS	*pDM1*	*DM1$^{G223A\ K224A\ H491V}$-2xHA*
pDT137	pGREENIIS	*pDM1*	*DM1^{G31R}-2xHA*
pDT138	pGREENIIS	*pDM1*	*DM1^{G31T}-2xHA*
pDT139	pGREENIIS	*pDM1*	*DM1^{G31D}-2xHA*
pDT140	pGREENIIS	*pDM1*	*DM1^{G31E}-2xHA*
pDT143	pGREENIIS	*pDM2d*	*DM2d^{T66A}-2xHA*
pDT144	pGREENIIS	*pDM2d*	*DM2d^{T66G}-2xHA*
pDT157	pGREENIIS	*pDM1*	*DM1$^{1-218}$-2xHA*
pDT158	pGREENIIS	*pDM2d*	*DM2d$^{1-254}$-4xMyc*
pDT164	pZZ006	*palcA*	*DM1$^{G223A\ K224A}$-2xHA*
pDT165	pZZ006	*palcA*	*DM1^{H491V}-2xHA*
pDT166	pZZ006	*palcA*	*DM1$^{G223A\ K224A\ H491V}$-2xHA*
pDT182	pGREENIIS	*pDM1*	*DM1$^{Col\text{-}0|495\text{-}988}$-2xHA*
pDT186	pGREENIIS	*pDM1*	*DM1^{H491T}-2xHA*
pDT187	pGREENIIS	*pDM2d*	*DM2d^{T541H}-4xMyc*
pDT192	pGREENIIS	*pDM1*	*DM1$^{1-528}$-2xHA*
pDT193	pGREENIIS	*pDM2d*	*DM2d/g (LRR swap 1)-4xMyc*
pDT194	pGREENIIS	*pDM2d*	*DM2d/g (LRR swap 2)-4xMyc*
pDT195	pGREENIIS	*pDM2d*	*DM2d/g (LRR swap 3)-4xMyc*
pDT196	pGREENIIS	*pDM2d*	*DM2d/g (LRR swap 4)-4xMyc*
pDT197	pGREENIIS	*pDM2d*	*DM2d/g (LRR swap 5)-4xMyc*
pDT198	pGREENIIS	*pDM2d*	*DM2d/g (LRR swap 6)-4xMyc*

pDT207	pGREENIIS	*pDM2d*	*TIR(DM2d)-NB(DM2d)-LRR(DM2g)-4xMyc*
pDT208	pGREENIIS	*pDM2d*	*TIR(DM2g)-NB(DM2g)-LRR(DM2d)-4xMyc*
pEC209	pGREENIIS	*pDM1*	*DM1-2xHA*
pEC300	pGWB420	*p35S*	*DM2d$^{1-358}$-10xMyc*
pMD324	pGREENIIS	*pDM2d*	*DM2d-2xHA*
pMD325	pGREENIIS	*pDM2d*	*DM2d-4xMyc*
pMD341	pGWB414**	*p35S*	*DM1$^{529-1067}$-3xHA*
pMD344	pGWB420	*p35S*	*DM1$^{687-1216}$-10xMyc*
pMD347	pGWB420	*p35S*	*DM2g-10xMyc*
pMD365	pGREENIIS	*pDM1*	*DM1$^{G223A\ K224A}$-2xHA*
pMD366	pGREENIIS	*pDM2d*	*DM2d$^{G259A\ K260A}$-4xMyc*
pMD444	pGREENIIS	*pDM1*	*DM1$^{1-308}$-2xHA*
pMD445	pGREENIIS	*pDM2g*	*DM2g-4xMyc*
pMD447	pGWB416	*pDM1*	*DM1-4xMyc*
pMD469	pGREENIIS	*pDM2d*	*DM2d^{T541V}-4xMyc*
pMD470	pGREENIIS	*pDM2d*	*DM2d^{T541D}-4xMyc*
pMD471	pGREENIIS	*pDM2d*	*DM2d$^{G259A\ K260A\ T541V}$-4xMyc*
pMD477	pGREENIIS	*pDM1*	*DM1$^{S34A\ H35A}$-2xHA*
pMD478	pGREENIIS	*pDM2d*	*DM2d$^{S69A\ H70A}$-4xMyc*

*pZZ006 incorporates ethanol-inducible AlcR transcription factor-*alcA* promoter system from *Aspergillus nidulans* [S17] into pMLBart binary backbone [S12].

**pGWB vectors are from [S10]

Oligonucleotide Primers for DM2d/DM2g Chimeras and Site-directed Mutagenesis

Primer	Purpose	Orientation	Sequence
G-38231	NB-ARC swap II	Forward	ATGAGATTGCTTGGGAAGTTACCTGCT TAGCTGGTAAACTCCCTTTGGGAT
G-38232	NB-ARC swap II	Reverse	ATCCCAAAGGGAGTTTACCAGCTAAGC AGGTAACTTCCCAAGCAATCTCAT
G-38233	NB-ARC swap II	Forward	TGAAGTGCTCAATGATGATACAATAGT AAGTTTTTTCA
G-38234	NB-ARC swap II	Reverse	TGAAAAAACTTACTATTGTATCATCATT GAGCACTTCA
G-38410	NB-ARC swap I	Forward	CACGAAGGTTTCGATGAGATTGCAAGG GAAGTTATGGCCCTTGCTGGTGAACTC CCTTTGGGATTGAAGGTTCTAGGC
G-38411	NB-ARC swap I	Reverse	GCCTAGAACCTTCAATCCCAAAGGGAG TTCACCAGCAAGGGCCATAACTTCCCT TGCAATCTCATCGAAACCTTCGTG
G-38412	NB-ARC swap I	Forward	GAAAGGGATATATGTGAAGTACTCGAT GACGATACAACAGTAAGTTTTTTCATTG CATCTC
G-38413	NB-ARC swap I	Reverse	GAGATGCAATGAAAAAACTTACTGTTG TATCGTCATCGAGTACTTCACATATATC CCTTTC
G-38521	TIR and LRR swap	Forward	CTAATGGATTCTTCTTTTTTCCTTGTCT TAGT
G-38522	TIR and LRR swap	Reverse	ACTAAGACAAGGAAAAAAGAAGAATCC ATTAG
G-38523	TIR and LRR swap	Forward	ATGGTTTTGTTGGGATGACACCTCATA TGG
G-38524	TIR and LRR swap	Reverse	CCATATGAGGTGTCATCCCAACAAAAC CAT
G-39654	LRR swap 1-6	Forward	CTTGATAATTGAGTTTATTTGATAAC
G-39655	LRR swap 1-6	Reverse	GTTATCAAATAAACTCAATTATCAAG
G-39656	LRR swap 1, 4	Forward	CTAAAGTAAGTAGTTTTGATGAAAACT
G-39657	LRR swap 1, 4	Reverse	AGTTTTCATCAAAACTACTTACTTTAG
G-39658	LRR swap 2, 5	Forward	GTCTCTAAGAAATTGTTCACGTGTTGT
G-39659	LRR swap 2, 5	Reverse	ACAACACGTGAACAATTTCTTAGAGAC
G-39660	LRR swap 3, 6	Forward	GCTAGAGACTCTTCCAATCAACATC

G-39661	LRR swap 3, 6	Reverse	GATGTTGATTGGAAGAGTCTCTAGC
G-39662	LRR swap 4, 5, 6	Reverse	GAATTGGGTAGCGGCCGCCCCCTCGAGC

Oligonucleotide Primers for qRT-PCR

Primer	Gene	Orientation	Sequence
N-0078	*TUB2*	Forward	GAGCCTTACAACGCTACTCTGTCTGTC
N-0079	*TUB2*	Reverse	ACACCAGACATAGTAGCAGAAATCAAG
G-13182	*PR1*	Forward	CGTTCACATAATTCCCACGA
G-13183	*PR1*	Reverse	AAGAGGCAACTGCAGACTCA
G-13184	*NPR1*	Forward	CGTTTCTCAGCAGTGTCGTC
G-13185	*NPR1*	Reverse	CCGTCTCACTGGTACGAAGA
G-38254	*WRKY46*	Forward	CGTGCATCTGTAATATGCTCTAGG
G-38255	*WRKY46*	Reverse	GATGATGGTCACTGCTGGAG
G-29987	*DM1-2xHA*	Forward	CCAAGTGGGCAACTTTGAAT
G-36197	*DM1-2xHA*	Reverse	AGCTGCATAGTCCGGGACGTC
G-23330	*DM2d-4xMyc*	Forward	CACCAAGCGAGCATGAGATA
G-31100	*DM2d-4xMyc*	Reverse	CTAAGCGCTACCGTTCAAGTCT

Supplemental References

S1. Bomblies, K., Lempe, J., Epple, P., Warthmann, N., Lanz, C., Dangl, J.L., and Weigel, D. (2007). Autoimmune response as a mechanism for a Dobzhansky-Muller-type incompatibility syndrome in plants. PLoS Biol. *5*, e236.

S2. Schreiber, K.J., Bentham, A., Williams, S.J., Kobe, B., and Staskawicz, B.J. (2016). Multiple domain associations within the Arabidopsis immune receptor RPP1 regulate the activation of programmed cell death. PLoS Pathog. *12*, e1005769.

S3. Hu, Z., Yan, C., Liu, P., Huang, Z., Ma, R., Zhang, C., Wang, R., Zhang, Y., Martinon, F., Miao, D., et al. (2013). Crystal structure of NLRC4 reveals its autoinhibition mechanism. Science *341*, 172-175.

S4. Kelley, L.A., Mezulis, S., Yates, C.M., Wass, M.N., and Sternberg, M.J. (2015). The Phyre2 web portal for protein modeling, prediction and analysis. Nat Protoc *10*, 845-858.

S5. Parker, J.E., Holub, E.B., Frost, L.N., Falk, A., Gunn, N.D., and Daniels, M.J. (1996). Characterization of *eds1*, a mutation in Arabidopsis suppressing resistance to *Peronospora parasitica* specified by several different *RPP* genes. Plant Cell *8*, 2033-2046.

S6. Tornero, P., Merritt, P., Sadanandom, A., Shirasu, K., Innes, R.W., and Dangl, J.L. (2002). *RAR1* and *NDR1* contribute quantitatively to disease resistance in Arabidopsis, and their relative contributions are dependent on the *R* gene assayed. Plant Cell *14*, 1005-1015.

S7. Tör, M., Gordon, P., Cuzick, A., Eulgem, T., Sinapidou, E., Mert-Turk, F., Can, C., Dangl, J.L., and Holub, E.B. (2002). Arabidopsis SGT1b is required for defense signaling conferred by several downy mildew resistance genes. Plant Cell *14*, 993-1003.

S8. Alonso, J.M., Stepanova, A.N., Leisse, T.J., Kim, C.J., Chen, H., Shinn, P., Stevenson, D.K., Zimmerman, J., Barajas, P., Cheuk, R., et al. (2003). Genome-wide insertional mutagenesis of *Arabidopsis thaliana*. Science *301*, 653-657.

S9. Clough, S.J., and Bent, A.F. (1998). Floral dip: a simplified method for *Agrobacterium*-mediated transformation of *Arabidopsis thaliana*. Plant J. *16*, 735-743.

S10. Nakagawa, T., Suzuki, T., Murata, S., Nakamura, S., Hino, T., Maeo, K., Tabata, R., Kawai, T., Tanaka, K., Niwa, Y., et al. (2007). Improved Gateway binary vectors: high-performance vectors for creation of fusion constructs in transgenic analysis of plants. Biosci. Biotechnol. Biochem. *71*, 2095-2100.

S11. Hellens, R.P., Allan, A.C., Friel, E.N., Bolitho, K., Grafton, K., Templeton, M.D., Karunairetnam, S., Gleave, A.P., and Laing, W.A. (2005). Transient expression vectors for functional genomics, quantification of promoter activity and RNA silencing in plants. Plant Methods *1*, 13.

S12. Zhao, Z., Andersen, S.U., Ljung, K., Dolezal, K., Miotk, A., Schultheiss, S.J., and Lohmann, J.U. (2010). Hormonal control of the shoot stem-cell niche. Nature *465*, 1089-1092.

S13. Box, M.S., Coustham, V., Dean, C., and Mylne, J.S. (2011). Protocol: A simple phenol-based method for 96-well extraction of high quality RNA from Arabidopsis. Plant Methods *7*, 7.

S14. Yu, S., Galvao, V.C., Zhang, Y.C., Horrer, D., Zhang, T.Q., Hao, Y.H., Feng, Y.Q., Wang, S., Schmid, M., and Wang, J.W. (2012). Gibberellin regulates the Arabidopsis floral transition through miR156-targeted SQUAMOSA promoter binding-like transcription factors. Plant Cell *24*, 3320-3332.

S15. Boyes, D.C., Nam, J., and Dangl, J.L. (1998). The *Arabidopsis thaliana RPM1* disease resistance gene product is a peripheral plasma membrane protein that is degraded coincident with the hypersensitive response. Proc. Natl. Acad. Sci. USA *95*, 15849-15854.

S16. Klodmann, J., Senkler, M., Rode, C., and Braun, H.P. (2011). Defining the protein complex proteome of plant mitochondria. Plant Physiol. *157*, 587-598.

S17. Caddick, M.X., Greenland, A.J., Jepson, I., Krause, K.-P., Qu, N., Riddell, K.V., Salter, M.G., Schuch, W., Sonnewald, U., and Tomsett, A.B. (1998). An ethanol inducible gene switch for plants used to manipulate carbon metabolism. Nat. Biotechnol. *16*, 177-180.